

" $^3\text{He}(p,p)^3\text{He}$ ANALYZING POWER AT 40.3 MeV"

BY

ALKIVIADIS C. ROUVAS

A THESIS

Submitted to the Faculty of Graduate Studies
in Partial Fulfillment of the Requirements
for the Degree of
MASTER OF SCIENCE

Department of Physics

University of Manitoba

Winnipeg, Manitoba



July 1986

Permission has been granted to the National Library of Canada to microfilm this thesis and to lend or sell copies of the film.

The author (copyright owner) has reserved other publication rights, and neither the thesis nor extensive extracts from it may be printed or otherwise reproduced without his/her written permission.

L'autorisation a été accordée à la Bibliothèque nationale du Canada de microfilmer cette thèse et de prêter ou de vendre des exemplaires du film.

L'auteur (titulaire du droit d'auteur) se réserve les autres droits de publication; ni la thèse ni de longs extraits de celle-ci ne doivent être imprimés ou autrement reproduits sans son autorisation écrite.

ISBN 0-315-33993-4

$^3\text{He}(\vec{p}, p)^3\text{He}$ Analyzing Power at 40.3 MeV

BY

ALKIVIADIS C. ROUVAS

A thesis submitted to the Faculty of Graduate Studies of
the University of Manitoba in partial fulfillment of the requirements
of the degree of

MASTER OF SCIENCE

© 1986

Permission has been granted to the LIBRARY OF THE UNIVERSITY OF MANITOBA to lend or sell copies of this thesis, to the NATIONAL LIBRARY OF CANADA to microfilm this thesis and to lend or sell copies of the film, and UNIVERSITY MICROFILMS to publish an abstract of this thesis.

The author reserves other publication rights, and neither the thesis nor extensive extracts from it may be printed or otherwise reproduced without the author's written permission.

Wer kann was Dummes, wer was Kluges denken,
das nicht die vorwelt schon gedacht?

*What wise or stupid thing can man conceive
that was not thought by nature in ages passed?*

FAUST

by J. W. von Goethe
(1749-1832)

ABSTRACT

Analyzing powers for proton elastic scattering from Helium-3 have been measured for proton scattering angles between 40 and 130 degrees. The angular distributions were determined for incident protons with a kinetic energy of 40.3 MeV. In order to perform the experiment a Helium-3 target was built and a nuclear detection system was designed. An optical pumping technique was used to polarize the target, using a Helium-4 discharge lamp. The preparatory work and the experiment were performed at the University of Manitoba Cyclotron Laboratory.

This study discusses the theory and the apparatus behind the nuclear orientation of Helium-3 by the optical pumping technique. The measurement of the nuclear polarization, the data collection system, the data analysis and the consistency of the results are discussed.

TABLE OF CONTENTS

ABSTRACT.....	i
TABLE OF CONTENTS.....	ii
LIST OF FIGURES.....	iv
LIST OF TABLES.....	ix
ACKNOWLEDGEMENTS.....	xi
I. INTRODUCTION.....	1
II. POLARIZATION METHOD OF HELIUM-3.	
A. INTRODUCTION.....	10
B. TARGET DESCRIPTION.....	13
C. METHOD AND THEORY.....	18
D. OPTICAL PUMPING INSTRUMENTATION.....	29
E. POLARIZATION MEASUREMENTS.....	37
III. SCATTERING EXPERIMENT.	
A. INTRODUCTION.....	43
B. CYCLOTRON FACILITY.....	45
C. BEAM LINE.....	49
D. SCATTERING CHAMBER.....	52
E. NUCLEAR DATA COLLECTION.	
i) Electronics.....	57
ii) Dead Time Corrections.....	62
iii) Nuclear Reactions in the Detector Material.....	62
iv) Measurement Procedure.....	62
v) Instrumental Asymmetries.....	63
F. OPTICAL DATA COLLECTION.....	67

IV. DATA ANALYSIS AND RESULTS.	
A. INTRODUCTION.....	73
B. PEAK AREA DETERMINATION.....	75
C. ANALYZING POWERS.....	78
D. INSTRUMENTAL AND MAGNETIC ASYMMETRIES.....	82
E. CONSISTENCY CHECKS.....	84
F. RESULTS AND ERROR ANALYSIS.....	91
V. CONCLUSION.	
A. HELIUM-3 POLARIZATION.....	96
B. HELIUM-3 ANALYZING POWERS.....	98
VI. REFERENCES.....	100

LIST OF FIGURES

FIGURE 1.1 Isobar diagram of the four nucleon system (from Fia73).

p. 2

FIGURE 1.2 Schematic diagram of an optical pumping apparatus and electronic level diagram. Atoms are polarized by the scattering of the circularly polarized resonant light. The transmitted light can be used to monitor the atomic polarization.

p. 7

FIGURE 2.1 Schematic diagram describing optical pumping of the metastable state of Helium-3 to polarize the ground state.

p.12

FIGURE 2.2 Target cell (dimensions in mm).

p.14

FIGURE 2.3 Energy levels in Helium-3.

p.19

FIGURE 2.4 Diagram of possible transitions between the 2^3S_1 ; $F=3/2$ and 2^3P_0 ; $F=1/2$ Helium-3 energy levels.

p.21

FIGURE 2.5 Isotope shift of the 1.083 micron line of helium.

p.24

FIGURE 2.6 Experimental layout of the apparatus for generating and measuring polarization.

p.30

FIGURE 2.7 Design details of the pumping lamps.

p.32

FIGURE 2.8 Detail of the pumping lamp and the polarizer, A = Lucite lens, B = Polarizer cemented between Fresnel lenses.

p.33

FIGURE 2.9 Weak discharge intensity dependence of the polarization.

p.39

FIGURE 2.10 Pumping light intensity dependence of the polarization.

p.40

FIGURE 2.11 Fluorescence signal as a function of the weak discharge intensity.

p.41

FIGURE 3.1 Duoplasmatron ion source and injection system.

p.47

FIGURE 3.2 General experimental area of the cyclotron laboratory.

p.48

FIGURE 3.3 Beamline B (30 degrees left) in experimental area B.

p.50

FIGURE 3.4 Scattering chamber (dimensions in mm).

p.53

FIGURE 3.5 Electronics diagram for one telescope. PA = preamplifier, SA = spectroscopy amplifier, TSCA = timing single channel analyzer, HV = high voltage supply, C = coincidence unit, LGS = linear gate and pulse stretcher, DSI = dual sum and inverter.

p.58

FIGURE 3.6 Timing diagram.

p.59

FIGURE 3.7 Online polarization apparatus.

p.68

FIGURE 3.8 Polarization as a function of time.

p.69

FIGURE 3.9 Diagram of the signals during a measurement cycle.

p.71

FIGURE 4.1 Illustration of the method for defining the background and determining the peak area.

p.76

FIGURE 4.2 The distribution of chi-square.

p.87

FIGURE 4.3 The distribution of consistency checks for K_m^2 .

p.88

FIGURE 4.4 The distribution of consistency checks for K_i^2 .

p.89

FIGURE 4.5 The distribution of consistency checks for K_p^2 .

p.90

FIGURE 4.6 Helium-3 Analyzing powers calculated at 40.3 MeV.

p.92

FIGURE 4.7 The Helium-3 Analyzing powers as calculated by Verheijen et al. at 25.0, 30.0, 32.5 and 35.0 MeV, and from this study at 40.3 MeV.

p.94

LIST OF TABLES

TABLE 1.1 Summary of polarizations for different Helium-3 targets.	p. 4
TABLE 2.1 Summary of methods presently used to measure Helium-3 nuclear orientation (from Dra84).	p.11
TABLE 2.2 Experimental details of the Helium-3 cells.	p.17
TABLE 2.3 Transition probabilities of Helium-3.	p.26
TABLE 3.1 Aperture dimensions (in mm).	p.60
TABLE 4.1 Definitions of formulae for the determination of the nuclear scattering asymmetries.	p.79

TABLE 4.2 Helium-3 Analyzing powers calculated at 40.3 MeV and asymmetries.

p.93

ACKNOWLEDGEMENTS

I would like to express my gratitude to my advisor, Dr. W.T.H. van Oers, whose guidance, advice, support and encouragement were most appreciated. His broad knowledge of nuclear physics was invaluable during the years I worked with him.

I am also indebted to Dr. R.H. McCamis, Dr. J. Birchall, Dr. P.J.T. Verheijen, and Mr. P. Drakopoulos for their help during the course of this study.

I wish to acknowledge the assistance of Mr. C. Haddock and Dr. J.S.C. McKee for their help with the I.B.M. computer, and also the assistance of Mr. G. Roy, Mr. I. Gusdal, Dr. C.A. Smith, Mr. J. Anderson, Mr. W. Mulholland, and Mr. D. Gallop.

Special thanks to my wife, Iris, whose patience, understanding and continuous encouragement during all the stages of this work cannot be sufficiently rewarded.

I wish to acknowledge the assistance of Dr. R. E. Brown, Dr. J. Campbell, Mr. M. Wango, Mr. W. M. Law, Mr. K. Chantziantoniou, and Miss. T. Eliyakut during the data collection. Finally, the assistance of Dr. G. S. Clark and Dr. N. T. Okumusoglu for reading this study.

I. INTRODUCTION

One of the fundamental problems of nuclear physics is the many body nuclear system. It has attracted considerable attention both experimentally and theoretically in the past, and will continue to do so in the future.

The main object of this problem is to learn more about the interactions between nucleons, thus gaining a better understanding of the world that surrounds us. For a long time the three-nucleon system has been the favored one among the few-nucleon systems. Its simplicity established it as the most suitable system for studying the details of the nucleon-nucleon forces in nuclei. Recent advances in the Faddeev[Fad61], three-nucleon formalism have produced very impressive results. It now seems feasible to begin extensive studies of the four-nucleon system.

A simple and direct method to study the four-nucleon system is the proton Helium-3 system which is currently the most appropriate way of studying the system of three protons and one neutron. The nucleus that can be formed from the above is Lithium-4. This is an unbound nuclear state and its ground state has been estimated to be 4.7 MeV above the energy of a Helium-3 particle plus a proton[Fia73]. Turning to figure 1.1 shows that, from low energy (less than 19 MeV) scattering data for proton Helium-3, four levels have been deduced to

FIGURE 1.1 Isobar diagram of
the four nucleon system (from
Fia73).

exist[Fia73]. Although a preliminary R-matrix analysis of higher energy scattering data indicated fluctuations in certain phase shifts[Bro78], no further trace of structure has been discovered above the four already existing levels.

The task of understanding the four-nucleon system is not an easy one, this study is a small contribution to it. The proton Helium-3 data are directly applicable to the charge conjugate system of a neutron plus tritium, assuming charge symmetry of nuclear forces. The unstable nature of both tritium and the neutrons makes experiments difficult compared to experiments using protons and Helium-3.

Data requiring a polarized Helium-3 target are difficult to obtain beyond 20 MeV, which is essential to establish the proton Helium-3 spin dependence needed in phase shift analyses, which are intermediate to a theoretical interpretation. The difficulty lies in the properties of the optical pumping technique used to polarize the Helium-3 and are due to low pressure (less than a few Pascals) and low polarization (less than 0.25). Table 1.1 summarizes the polarizations for different polarized Helium-3 targets. Beyond 20 MeV the elastic differential cross section decreases rapidly as the energy increases and the background scattering becomes a problem[Ver84]. Recent developments of laser technology may allow the replacement of the Helium-4 discharge lamps with more intense lasers. Laloe et al.[Lal85], reported polarizations up to 0.70 by pumping gas with a color center laser. The color center laser is excited by a dye laser

Values for P_p^2 on different polarized ^3He targets

Polarization P	Pressure p (Pa)	P_p^2 (Pa)	Reference
0.093	530	5	Bak69
0.105	530	6	McS70
0.15	530	12	Bak71
0.22	530	26	Roh71
0.16	200	5	Tim71a
0.10	600	6	Bec75
0.165	530	14	War75
0.18	270	9	Mul78
0.22	530	26	Sza78
0.38	400	58	Nac82
0.13	647	11	Ver83
0.12	475	7	This work

TABLE 1.1 Summary of polarizations for different Helium-3 targets.

emitting in the infrared around the wavelength $\lambda = 890$ nm, the dye laser is itself pumped by the red lines ($\lambda = 644$ and $\lambda = 690$ nm respectively) of a Krypton laser. The pumping light is delivered at 1.08 micrometers, circularly polarized by a quarter wave plate and sent onto the Helium-3 cell along the magnetic field axis (B_0). Schmor et al. [Sch84], reported results for polarized Hydrogen of 0.80 to 0.90 using a dye laser. Optical pumping is performed by a broadband coherent dye laser operating at 5896 angstroms. Broadband pumping is formed from circularly polarized beams. Splitting the laser beam into two and pumping the sodium bi-directionally increases the polarization. The laser is operating on several modes, each much narrower than the Doppler width, averaging in time to a 30 GHz total bandwidth. Each narrow mode interacts with a population of sodium atoms having velocity $+v$. By pumping from the other direction, a particular mode will also interact with atoms having velocity $-v$. The polarization is measured using the Faraday rotation technique.

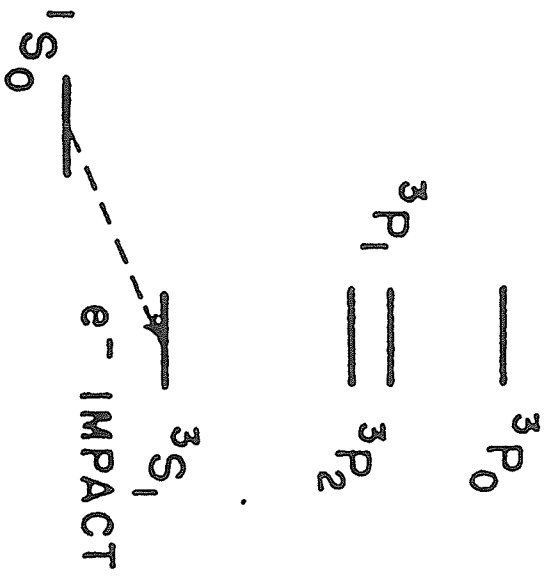
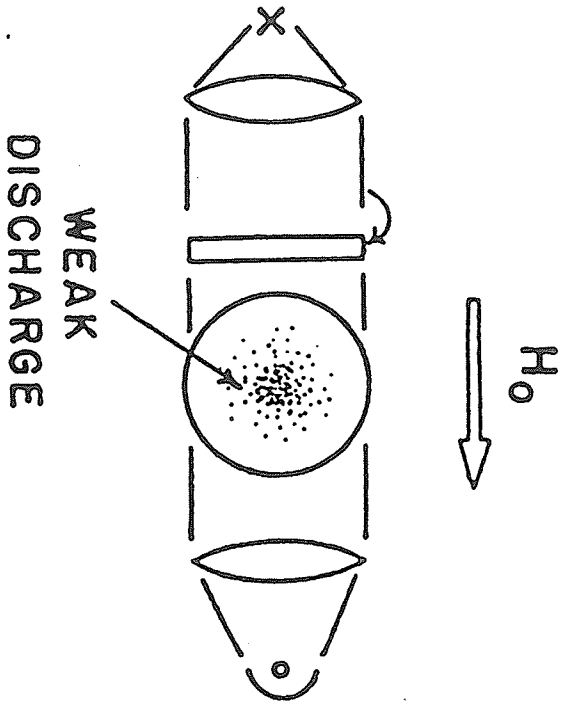
At the University of Manitoba a substantial program of measurements has been undertaken in the energy range between 20 and 50 MeV. This program has already completed measurements of total cross sections [Sou76], differential cross sections [Bro80; Mur84], proton analyzing powers [Bir84], as well as Helium-3 analyzing powers [McC85]. This work reports on the measurements of Helium-3 analyzing powers at 40.3 MeV using an unpolarized proton beam incident on a polarized Helium-3 target.

Helium-3 analyzing powers below 20 MeV have been measured by Szaloky et al.[Sza78], at five energies between 2.3 and 8.8 MeV, as twelve point angular distributions, by McSherry et al.[McS70], at nine energies from 3.8 to 10.9 MeV, as four point angular distributions, and by Baker et al.[Bak71], at 19.4 MeV as an eighteen point angular distribution. Measurements for energies higher than 20 MeV were obtained by Muller et al.[Mul78], at 25.0 MeV as a nine point angular distribution. The energy dependence was reported at a fixed lab angle of 135 degrees for five energies between 19.6 and 26.5 MeV[Mul78], Ware et al.[War75]. measured a fourteen point angular distribution at 26.0 MeV and McCamis et al.[McC85], measured from 25.0 to 35.0 MeV twelve point angular distributions.

In the present study a polarized Helium-3 target was an important part of the experiment. The technique used to polarize the target was by optical pumping using Helium-4 lamps[Col60], thus imposing the limitations of low pressure and low polarization. Optical pumping refers to the technique that uses light to produce a redistribution of atoms among states. This is not a direct technique, as the metastable 2^3S_1 state serves as a ground state in this case.

The polarization was achieved by placing the Helium-3 gas filled target inside a uniform magnetic field. The magnetic field, in turn, was produced by a pair of Helmholtz coils, strong enough to define a clear quantization axis (Figure 1.2). A number of 2^3S_1 metastable atoms were created inside the Helium-3 gas filled target by means of a

FIGURE 1.2 Schematic diagram of an optical pumping apparatus and electronic level diagram. Atoms are polarized by the scattering of the circularly polarized resonant light. The transmitted light can be used to monitor the atomic polarization.



weak discharge. The metastable atoms were pumped to the 2^3P_0 state by the infrared component of the Helium-4 lamp at a wavelength of 1.083 micrometers which corresponds to the $2^3S_1 - 2^3P_{0,1,2}$ transition of Helium-3[Col60]. The optical power output of these lamps is about 10^{18} infrared photons per minute and is achieved through a radiofrequency excitation to avoid Doppler broadening of the emission lines[Dan71c].

With reference to the circularly polarized pumping light, the transition from the 2^3S_1 state obeys the selection rule ($\Delta M=-1$) for positive and ($\Delta M=+1$) for negative helicity light. The atoms remain in the excited state for a small period of time and then decay back to the 2^3S_1 metastable state. During the cycle the effect is the transfer of the angular momentum of the photons to the triplet metastable atoms. Due to the hyperfine coupling of nuclei and electrons, the orientation of the electronic angular momentum is transferred to the nuclear spin. During this process the atoms collide with the ground state, exchanging electronic clouds, the spin remains unaffected and the nuclear polarization is transferred to the ground state atoms[Dan71b].

A discussion of the polarization instrumentation is included in chapters II and III, where preparatory measurements and the measurements of nuclear polarization are described. The details of the nuclear instrumentation and of the data collection system are discussed in chapter III. The experiment was performed at the

University of Manitoba Cyclotron Laboratory using a proton beam energy of 40.4 MeV from the sector focussed cyclotron.

Analysis of the data collected, the results, error analysis and consistency of the results are discussed in chapter IV.

Finally, chapter V is a summary of the previous sections and addresses future developments and improvements.

CHAPTER II

POLARIZATION METHOD

A. INTRODUCTION

The determination of nuclear polarization in a Helium-3 gas filled target is a vital part of the experiment and special care must be taken to avoid systematic error in its measurement due to instrumental imperfections.

There are several ways to detect nuclear polarization, which arise from two techniques (Table 2.1). One method is the use of the "nuclear magnetic resonance" technique. It involves a direct detection, and employs the 1^1S_0 ground state for the detection of nuclear polarization. The other method refers to "optical methods" (probing beam, fluorescence, and pumping light monitoring) which so far has given acceptable results in similar studies. In our study the fluorescence technique was employed. It is not a direct technique of detection. The intensity of the pumping light that is absorbed by atoms in the 2^3S_1 metastable state and subsequently reemitted at right angles to the applied magnetic field (Figure 2.1) is measured.

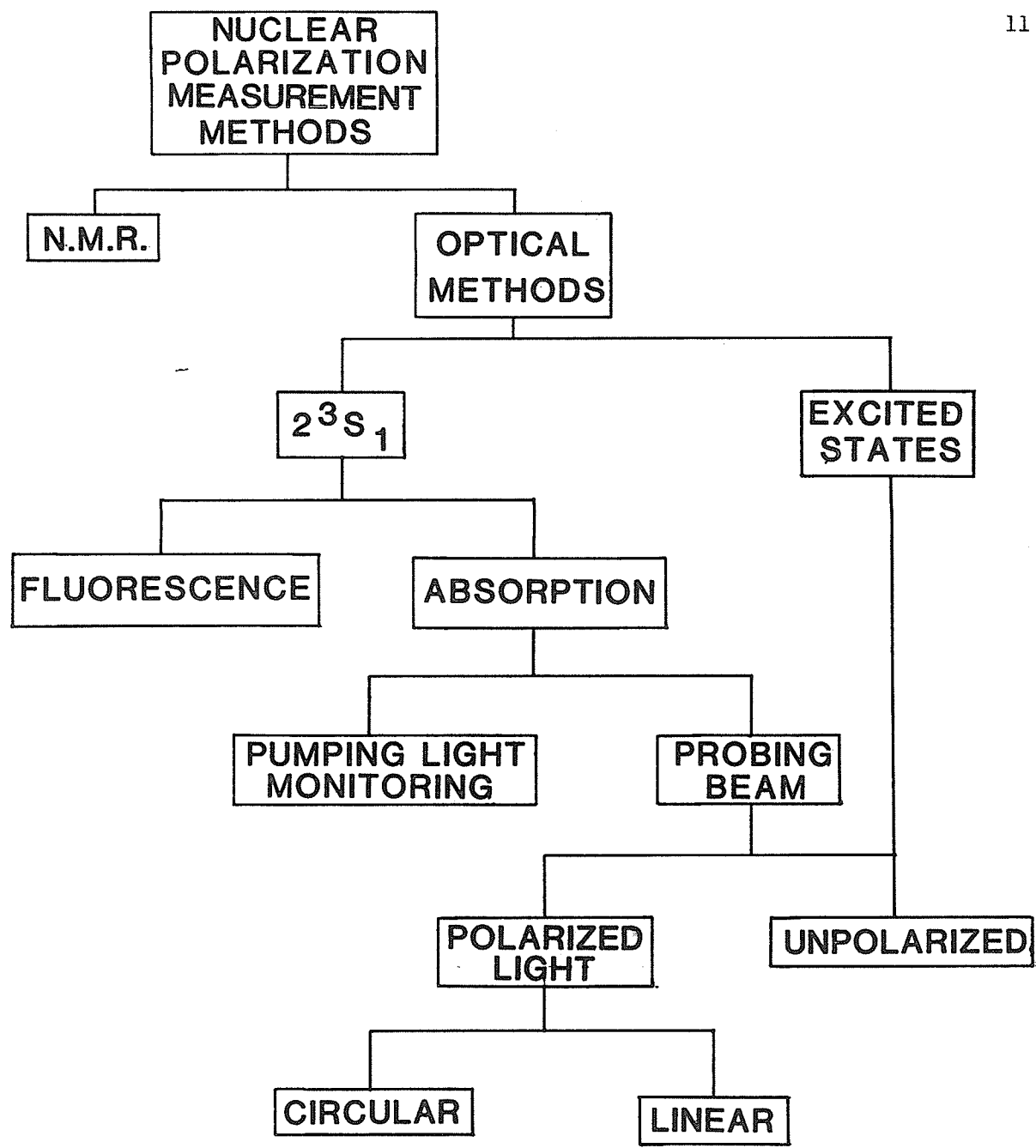
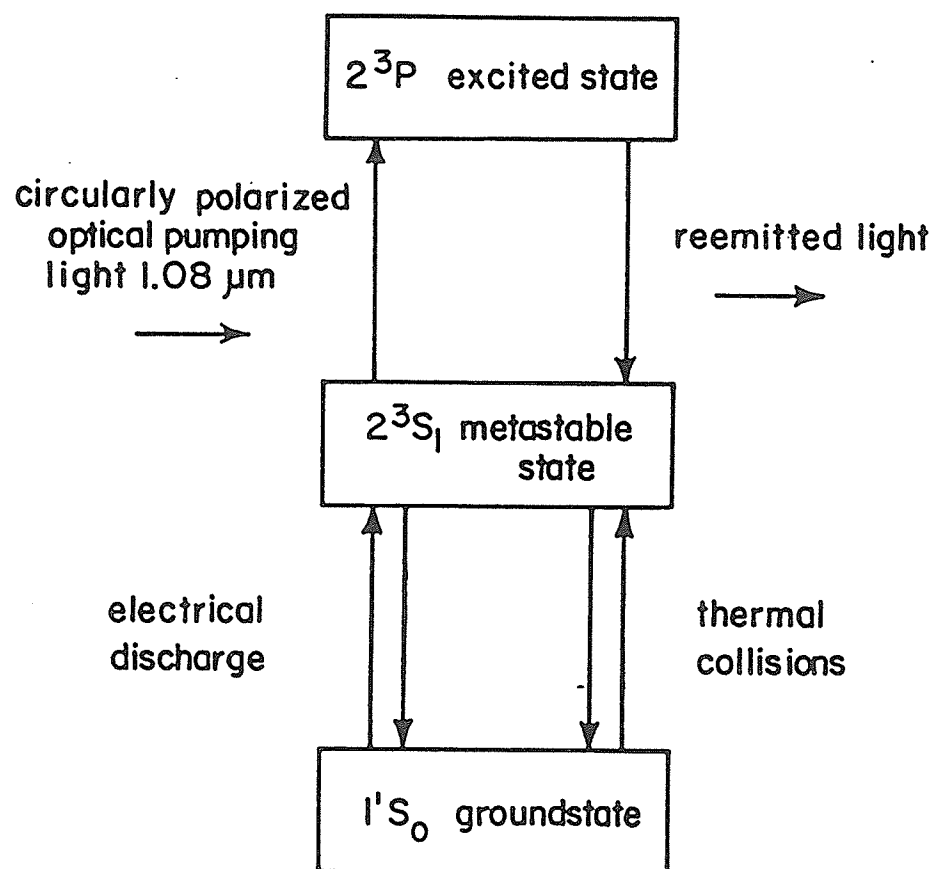


TABLE 2.1 Summary of methods presently used to measure Helium-3 nuclear orientation (from Dra84).

FIGURE 2.1 Schematic diagram
describing optical pumping of the
metastable state of Helium-3 to
polarize the ground state.

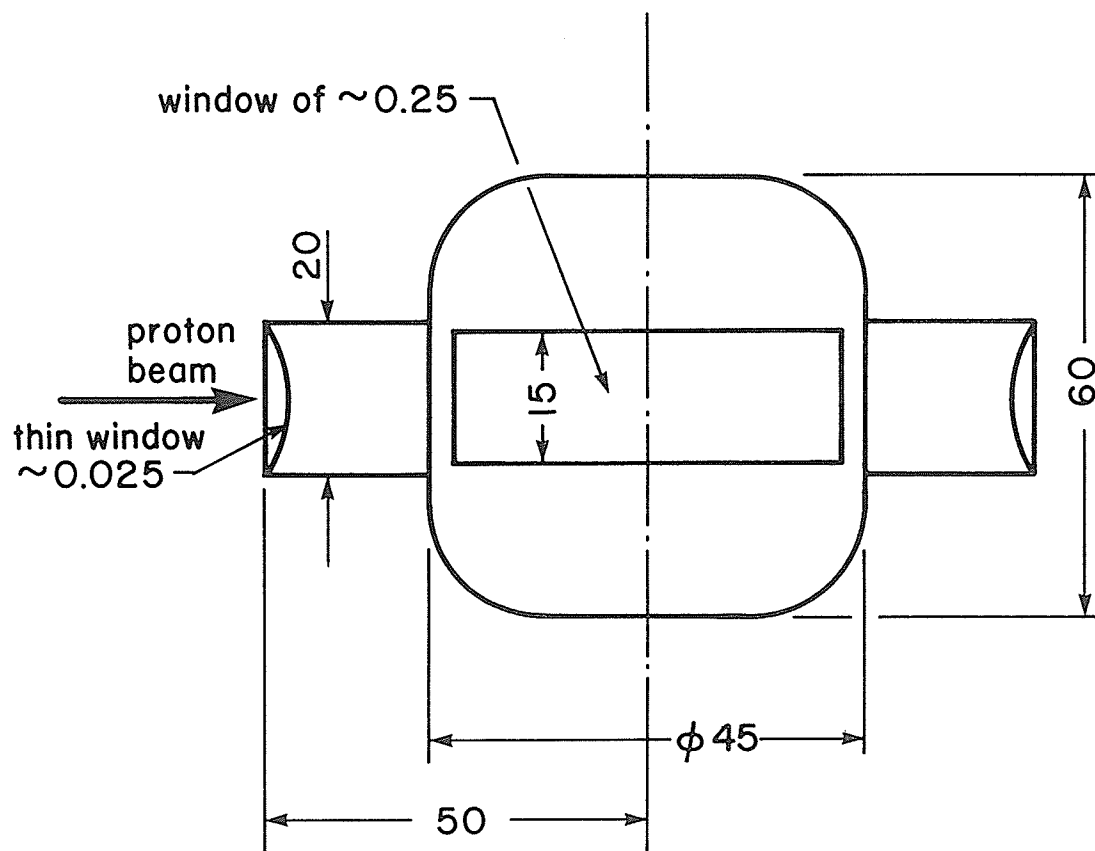


B. TARGET DESCRIPTION

The design and construction of the Helium-3 gas filled cell was undertaken at the University of Manitoba by Verheijen[Ver83]. The material used at the beginning of the study was type 1720 Corning glass. The advantages of No.1720 glass are the following. First, the permeation at room temperature of helium through this material is lower than for ordinary pyrex glass (Corning data sheets). Secondly, the ground state relaxation time due to helium atom collisions with the walls of the cell is better than for ordinary pyrex glass[Tim71a]. However, there is one disadvantage as No.1720 glass has a high softening point, and is therefore difficult to handle. Another disadvantage is that its lifetime is limited due to proton beam irradiation causing the windows to develop pinholes at the seal. Finally, standard laboratory pyrex glass No.7740 was used. It proved to be a good substitute and prolonged the lifetime of the cells. When not in use the filled Helium-3 cells were stored in a refrigerator at -20 degrees C.

The Helium-3 cells consisted of a thin walled cylindrical glass bulb of 57 mm diameter and 60 mm height, filled with an average of 0.475 kPa (3.6 Torr) of Helium-3 of 99.995% purity (Figure 2.2). In each cell there are two extensions of 31 mm length with a 0.03 mm thin window at the end. On the outer perimeter of the cylindrical bulb two windows have been developed which were etched to a thickness of 0.25

FIGURE 2.2 Target cell
(dimensions in mm).



mm. This reduces the energy loss for protons scattered from the Helium-3 nuclei. The extensions are in such positions as to minimize the effects of double scattering through large angle scattering from the beam exit point, and small angle scattering when the beam passes the entrance window. Before filling the cells an extensive cleaning procedure was undertaken in order to improve their quality. The cleaning process involved the use of dilute hydrofluoric acid (10%) for a period of less than a minute followed by distilled water to remove the acid and, as a final step, acetone was used to remove the water droplets. The clean cells were placed under vacuum, which was produced by a three stage oil diffusion pump and a supporting roughing pump. The cells were then placed in a furnace where the vacuum was continued at a constant pressure of 10^{-5} Pa (10^{-7} Torr) and were baked at a temperature of 280 degrees C for several days. The cells were cleaned by means of a discharge (Tesla coil) and filled at the desired pressure with Helium-3 gas, through a quartz diffusion element to avoid contamination[Ver83]. In addition, some external parts of the target were coated with a special black paint to avoid stray light before being placed in the scattering chamber.

The pressure of the cells was also calculated from the experimental results using an analysis described by Verheijen[Ver83]. The analysis was made using the cross section at the energy of 40 MeV as given by Sourkes et al.[Sou76], the number of particles of the beam (collected as charge in the Faraday cup), the geometry factor as described by Silverstein[Sil59] and the left and the right yields from

our experiment at the corresponding cycle.

The cells used in this experiment had an average pressure of 0.475 kPa (3.5 Torr) and a typical polarization of 0.12 ± 0.01 , (Table 2.2) which is consistent with other studies (Table 1.1).

Data relevant to the target cells used in
this experiment

Cell	Pressure (Pa)	Polarization	Runs
E14	494	0.12	45,46,47, 48,49.
E36	658	0.14	50,51,52, 53,54,55, 56,57,58, 59.
E41	273	0.10	60,61.

TABLE 2.2 Experimental details of the Helium-3 cells.

C. METHOD AND THEORY

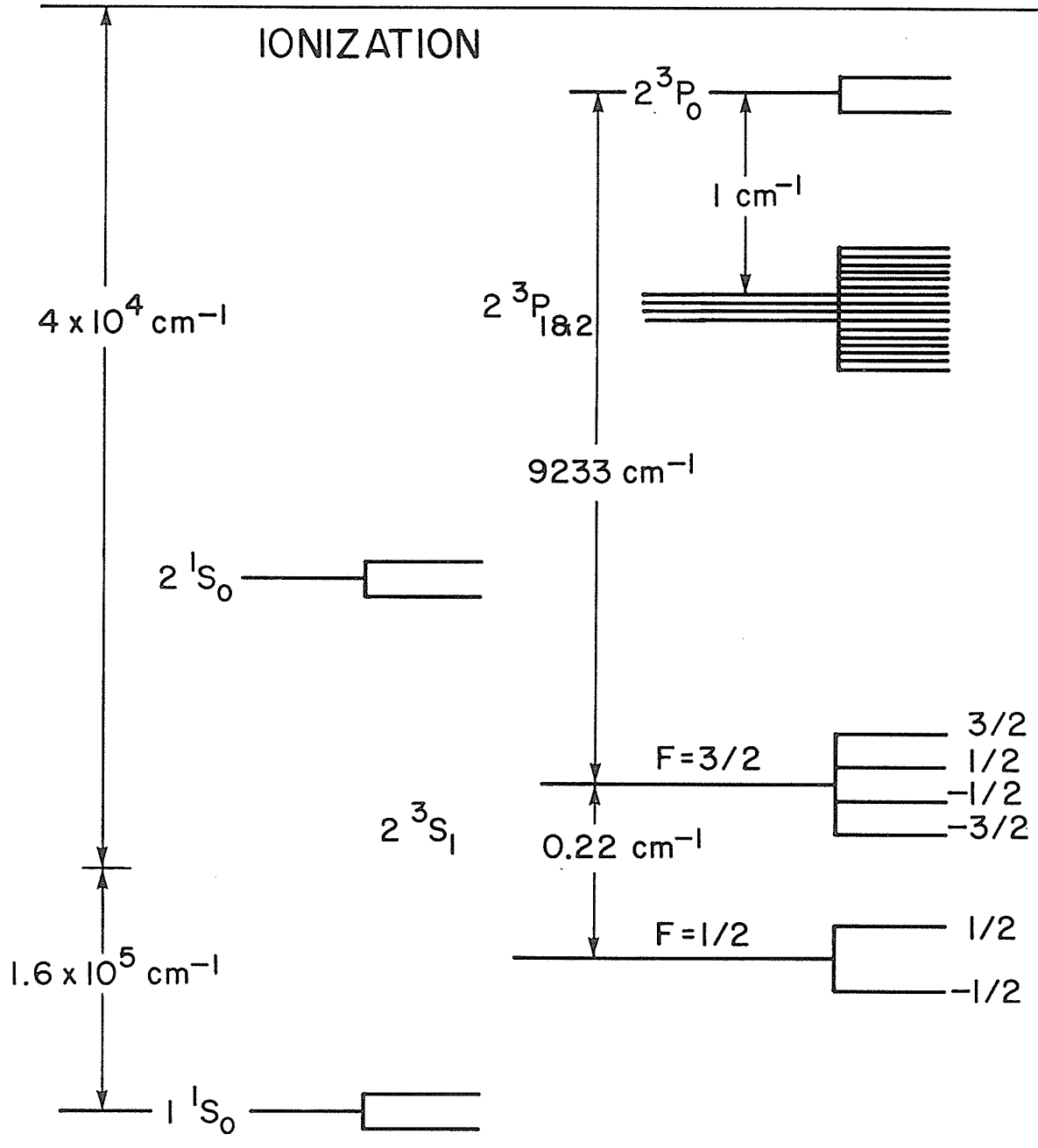
The nuclear orientation of Helium-3 by optical pumping is a well known and often used technique. Colegrove et al. [Col63], first polarized Helium-3 (2^3S_1) and ground state Helium-3 by optical pumping.

Optical pumping is a powerful method to create and to maintain a non-equilibrium population of atoms in different quantum states. These can be states of different energy, different fine structure levels (J), different hyperfine quantum number (F), or different Zeeman sublevels (m_I, m_J, m_F). In the latter case we achieve nuclear orientation.

A description in detail of the nuclear orientation process in Helium-3 ($I=1/2$) involves, first the process of "optical pumping" and second, the distribution of angular momentum among the atoms in the energy levels of Helium-3 (Figure 2.3).

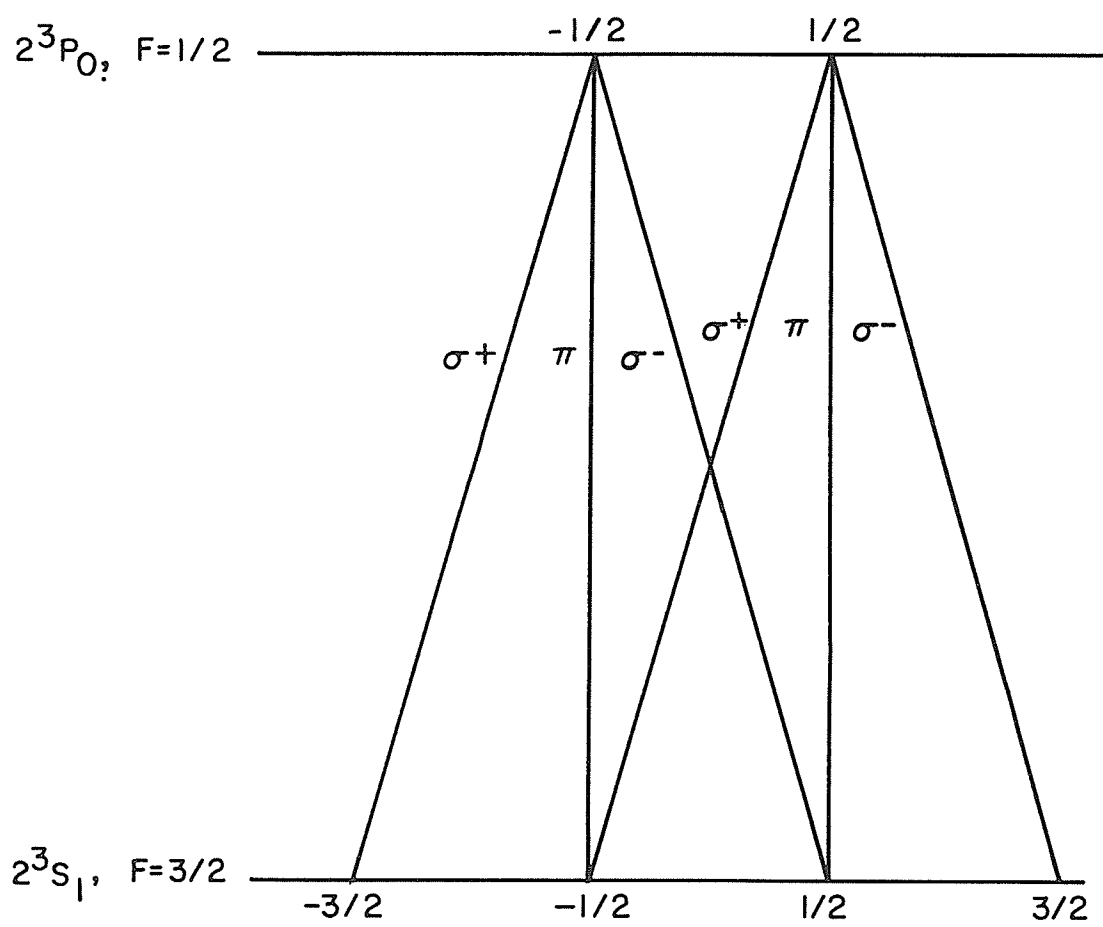
Optical pumping limits us to long lived states such as transitions between the ground state (1^1S_0) to either the singlet metastable state (2^1S_0), or to the triplet metastable state (2^3S_1). Due to parity conservation no transitions between the triplet and the singlet metastable states are allowed. In the optical pumping technique which is used in this work, a cell containing

FIGURE 2.3 Energy levels in
Helium-3.



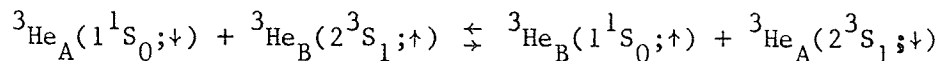
Helium-3 is placed in a magnetic field. A weak electrical discharge is struck in the gas, populating both metastable states with a density of $10^{10} - 10^{12}$ atoms/cm³. The lifetime of the metastable atoms is mainly determined by atomic collisions with impurities and container walls and is of the order of 10^{-5} sec [Tim71b]. The decay from the excited states (P) to any of the lower states (S) is determined by transition probabilities, and in all cases more than 90% of the decay goes to the lowest state [Ver83]. Circularly polarized 1.083 micrometers wavelength light from a Helium-4 lamp is directed along the magnetic field into the cell. The metastable Helium-3 atoms are excited only from the $2^3S_1; F=3/2$ to the $2^3P_0; F=1/2$ state (Figure 2.4), because of a chance coincidence between the Helium-4 and Helium-3 lines. If right handed circularly polarized light is used, only the $2^3S_1; F=3/2, m_F=-3/2 \rightarrow 2^3P_0; F=1/2, m_F=-1/2$, and $2^3S_1; F=3/2, m_F=-1/2 \rightarrow 2^3P_0; F=1/2, m_F=1/2$ transitions are induced. If the lower $2^3S_1; F=1/2$ levels were not present, the excited atoms would decay back to the four sublevels of the $2^3S_1; F=3/2$ and the atomic population in each level would be altered. In the absence of relaxation mechanisms, the atoms would accumulate in the sublevel of $2^3S_1; F=3/2$ state, and thus acquire a net total angular momentum. The presence of the lower $2^3S_1; F=1/2$ state reduces the amount of angular momentum which can be acquired since the atoms which decay to the $2^3S_1; F=1/2, m_F=-1/2$ are isolated from the pumping light and cannot be transmitted to the $2^3P_0; F=1/2, m_F=1/2$ level by the absorption of a circularly polarized photon.

FIGURE 2.4 Diagram of possible
transitions between the 2^3S_1 ;
 $F=3/2$ and 2^3P_0 ; $F=1/2$ Helium-3
energy levels.



Under the conditions of a weak discharge the metastable 2^3S_1 atom population constitutes only 10^{-6} of the total numbers of atoms, most of which are in the 1^1S_0 ground state. While in the 2^3S_1 state, a helium atom collides elastically with the ground state atoms. These collisions do not cause any significant disorientation of polarized atoms in the metastable state (collision time 10^{-13} sec, so spin $I=1/2$ remains unaffected)[Col60].

The orientation of the nucleus originally polarized in the metastable atom is unaffected by the collision, and the nuclear orientation is produced in the ground state atom population through the de-excitation of 2^3S_1 atoms. The collisions can be described as follows:



where A and B indicate two individual atoms, and the arrows refer to the direction of the nuclear spin.

Polarization is measured by optical absorption. The optical method is best suited for low pressure measurements[Bec77], where polarization is deduced from the metastable pumping light absorption, since the metastable excitation transfer maintains the ground state and metastable polarizations equal.

Let us assume that the populations of the two sublevels of the ground state are N_1 and N_2 , then the nuclear polarization P in this state is defined as:

$$P = \frac{N_1 - N_2}{N_1 + N_2} \quad (\text{II.1})$$

Anderson et al.[And60], have developed the general forms of the steady-state solution for spin exchange problems in which the relaxation times of the spin systems are much longer than the interaction time. In our case, the population levels were obtained in terms of the ground state polarization by the ratio:

$$\frac{n(-3/2)}{n(-1/2)} = \frac{n(-1/2)}{n(1/2)} = \frac{n(1/2)}{n(3/2)} = \frac{N_1}{N_2} = \frac{1 + P}{1 - P} \quad (\text{II.2})$$

A condition is that[And60]:

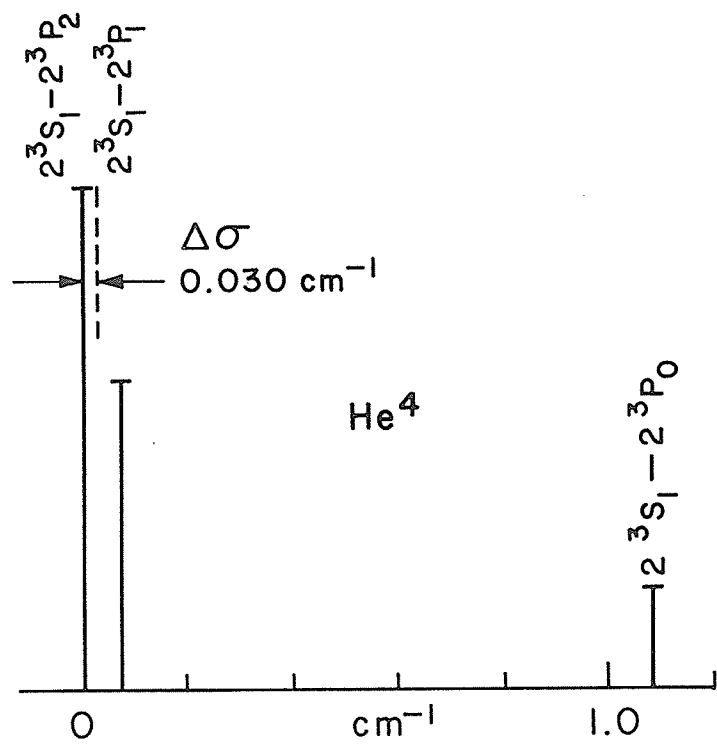
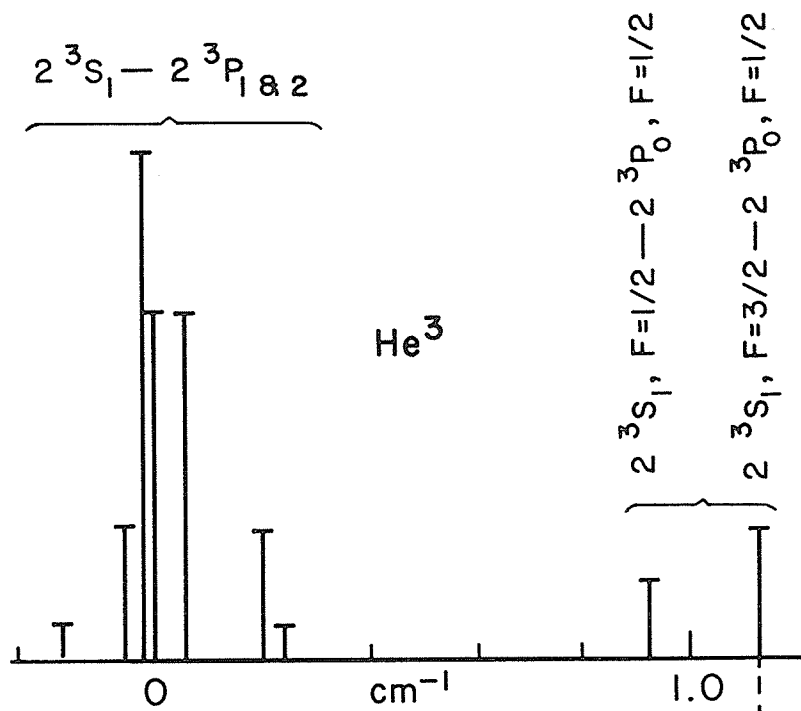
$$n(-3/2) + 2n(-1/2) + 2n(1/2) + n(3/2) = n \quad (\text{II.3})$$

and:

$$\begin{aligned} n(-3/2) &= \left(\frac{(1-P)^3}{(6+2P^2)} \right) n \\ n(-1/2) &= \left(\frac{(1+P)(1-P)^2}{(6+2P^2)} \right) n \\ n(1/2) &= \left(\frac{(1+P)^2(1-P)}{(6+2P^2)} \right) n \\ n(3/2) &= \left(\frac{(1+P)^3}{(6+2P^2)} \right) n \end{aligned} \quad (\text{II.4})$$

where n is the population of the triplet state and the $n(i)$ are the populations of 2^3S_1 magnetic sublevels (Figure 2.5).

FIGURE 2.5 Isotope shift of
the 1.083 micron line of helium.



It has already been mentioned that the pumping light is circularly polarized, thus only $\Delta M=+1$ transitions can be excited. If the helicity is assumed to be negative, then only the appropriate magnetic sublevels of the two hyperfine components can absorb radiation. If the gas is optically thin, the absorption of radiation is linear and the flux will be:

$$I(P) \propto f\{n(-3/2)a\} + \{b+c(1-f)n(-1/2)\} \quad (\text{II.5})$$

where $a, b,$ and c are the absorption probabilities of the transitions (Table 2.3) that originate from the $F=3/2$ and $F=1/2$ (D_0) levels which are assumed be equally illuminated [Sch65]. The constant f describes the relative absorption of the $F=3/2$ hyperfine component. Timsit et al. [Tim71a], found that the separation of the $2^3S_1 - 2^3P_2$ line emitted from a Helium-4 discharge lamp and the $2^3S_1; F=3/2 - 2^3P_0; F=1/2$ absorption line of Helium-3 is only 0.03 cm^{-1} . The value of the constant f is clearly governed by the Doppler broadening of the Helium-4 lamp emission lines. Colegrove et al. [Col63], assumed that $f=1/2$, while Greenhow [Gre64], found that the absorption was due only to the $F=3/2$ hyperfine component and consequently used $f=1$. Recently Timsit et al. [Tim71a], obtained absorption that was almost gaussian, due to the $F=3/2$ line, and verified Greenhow's results [Gre64]. In our study f was assumed to be equal to unity, since our lamps were identical to the ones described by Daniels and Timsit.

2^3S_1 $F=3/2$	2^3P_0	
	$m_F=1/2$	$m_F=-1/2$
$m_F=3/2$	1 σ^-	0 -
$m_F=1/2$	2/3 π	1/3 σ^-
$m_F=-1/2$	1/3 σ^+	2/3 π
$m_F=-3/2$	0 -	1 σ^+

TABLE 2.3 Transition probabilities of Helium-3.

Colegrove et al.[Col63], developed the ideas and Greenhow[Gre64], adapted them (by a combination of equations II.4 and II.5), and related the polarization P to the light absorbed by the metastables:

$$\frac{I(0) - I(P)}{I(0)} = \frac{P(15 - 10P + 3P^2)}{(6 + 2P^2)} \quad (\text{II.6})$$

where $I(0)$ is the light absorbed by an unpolarized sample and $I(P)$ is the light absorbed by a sample having polarization P . This equation is applied to the resonance radiation from a Helium-4 lamp incident on a Helium-3 sample, where due to the isotope shift, only the D_0 line of Helium-3 is illuminated. Colegrove et al.[Col63], after considering the absorption coefficients and collisional mixing in the 2^3P states in detail, concluded that it leads to more efficient pumping than in the case of a Helium-3 lamp exciting both D_0 and D_3 transitions.

Daniels et al.[Dan71a], proposed a variation of equation (II.6). This equation takes into account the fact that pumping can also excite σ^- and π transitions due to imperfections such as stray light noise:

$$\frac{I(0) - I(P)}{I(0)} = \frac{(15P - 10P^2 + 3P^3)R_+ - (15P + 10P^2 + 3P^3)R_- + 8P^2R_0}{2(3 + P^2)(R_+ + R_- + R_0)} \quad (\text{II.7})$$

where R_+ , R_- , and R_0 are constants determined from the geometrical characteristics of the pumping lamp and are, respectively, proportional to the transition rates for σ^+ , σ^- , and π transitions induced in unpolarized Helium-3. R_+ is related to right handed

(negative helicity), R_- is related to left handed (positive helicity) and R_0 is related to the angle of incidence of the light on the target. In ideal conditions these constants are normalized to unity ($R_+=1, R_-=R_0=0$) thus equation (II.7) reduces to equation (II.6). Determination of the above constants is rather complicated. A disadvantage of this method is that the obtained signal is not related directly to the 2^3S_1 state but to the excited state [Dra84].

D.OPTICAL PUMPING INSTRUMENTATION

The instrumental layout for the optical pumping of Helium-3 is similar to that developed by the Toronto group [Tim71a]. A typical set up includes; i) the Helium-3 gas cell, ii) the Helium-4 filled pumping lamps, iii) Helmholtz coils capable of producing a uniform magnetic field and, iv) various instruments such as, a 6 A power supply for the Helmholtz coils, a 1 MHz oscillator for cell discharge and a 150 MHz oscillator for the Helium-4 discharge lamps (Figure 2.6).

i) Helium-3 cells

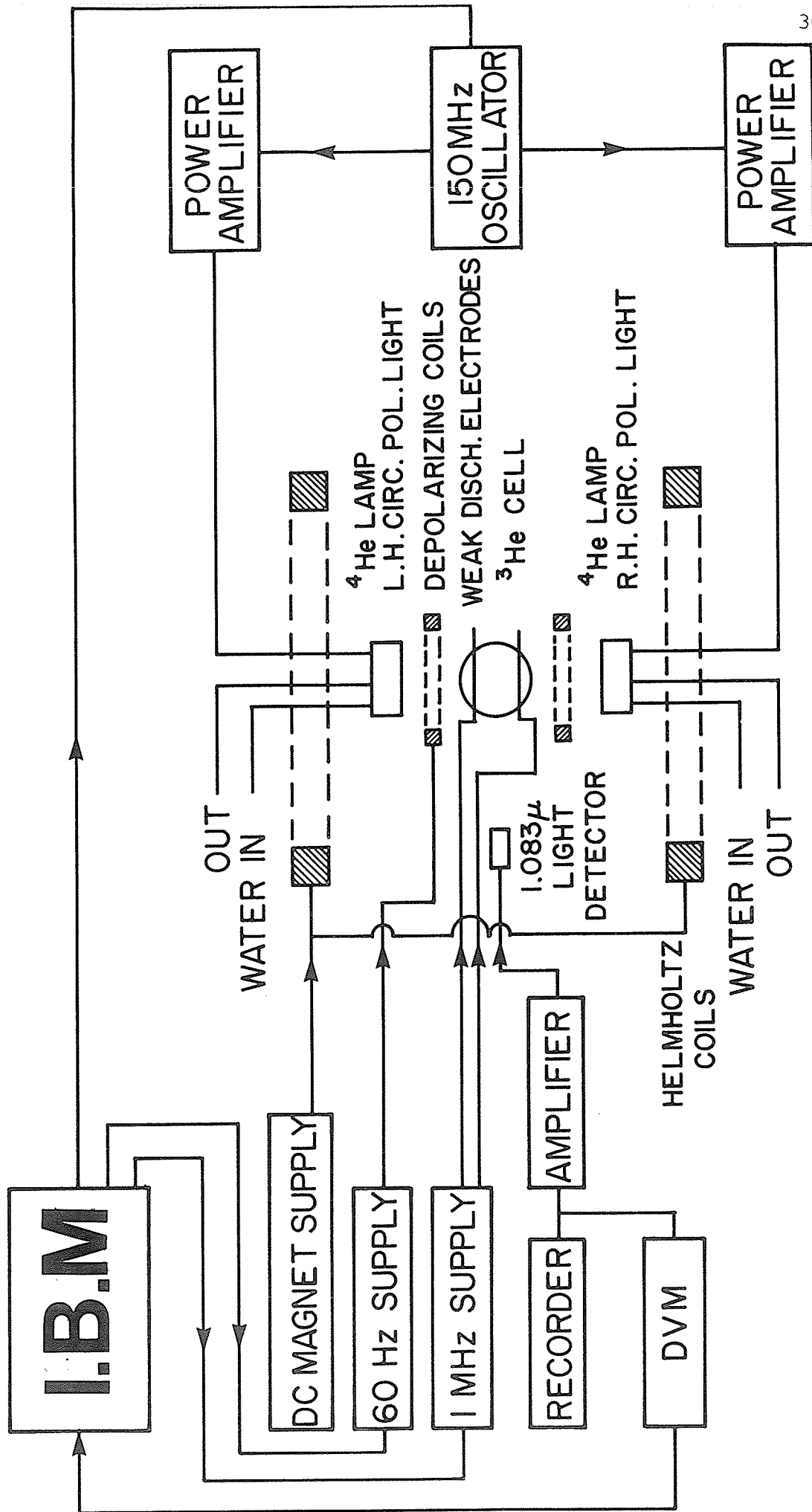
The cells were constructed at the University of Manitoba by Verheijen [Ver83]. A detailed description is given in section B of this chapter.

ii) Pumping light source

The aim of the light source in this experiment was to provide an intense parallel beam of circularly polarized light with a narrow spectral line width.

The light source consists of the Helium-4 filled lamp, and a circular polarizer sandwiched between two Fresnel lenses. The pumping lamps are similar to the ones built by the Toronto group [Dan71c]. The body of each lamp is made of quartz and the light is produced in the

FIGURE 2.6 Experimental layout
of the apparatus for generating and
measuring polarization.



constricted part of its body, which is 20 mm x 20 mm x 1 mm thick. The latter part was constructed in such a manner as to satisfy optical requirements and to prevent build up of sputtered material on the walls of the constriction. The discharge tube is surrounded by a cooling jacket, made out of pyrex glass, through which the cooling fluid is circulated. Water cooling is provided by a continuous flow around the electrodes and plasma area. 38% of the 1.083 micron light is absorbed in the 29 mm of water between the constriction and the collector lens of the lamp (Figure 2.7 and Figure 2.8).

The electrodes are made of tungsten and have a molybdenum cap to minimize gaseous impurities [Tim70]. A lucite collecting lens is attached at the bottom side of the lamp with ordinary silicon grease (General Electric).

Prior to use, the lamps were internally cleaned, for better performance, using dilute hydrofluoric acid (10%), distilled water and acetone. This procedure was repeated several times to remove the sputtering residuals from the plasma area of the discharge tube. Then, the lamp was internally cleaned by means of discharge, which was accomplished by first pumping out the lamp to a pressure near 1.3 Pa (0.1 Torr), admitting a new sample of Helium-4 gas into the body of the discharge tube at a low pressure, and then tuning on the R.F. oscillator through a pi network. The Helium-4 gas contaminated by the impurities was then pumped out and the cycle repeated. The cycle needed to be repeated four or five times for the spectrum of the light

FIGURE 2.7 Design details of
the pumping lamps.

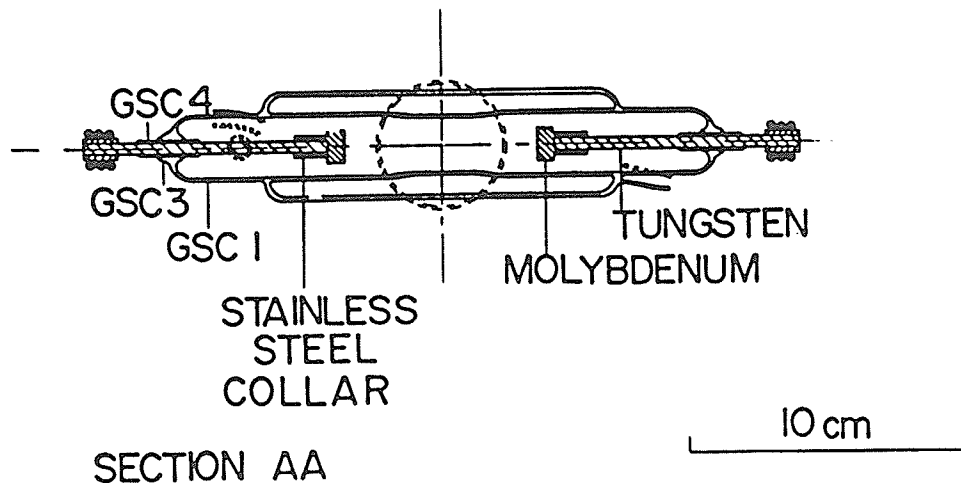
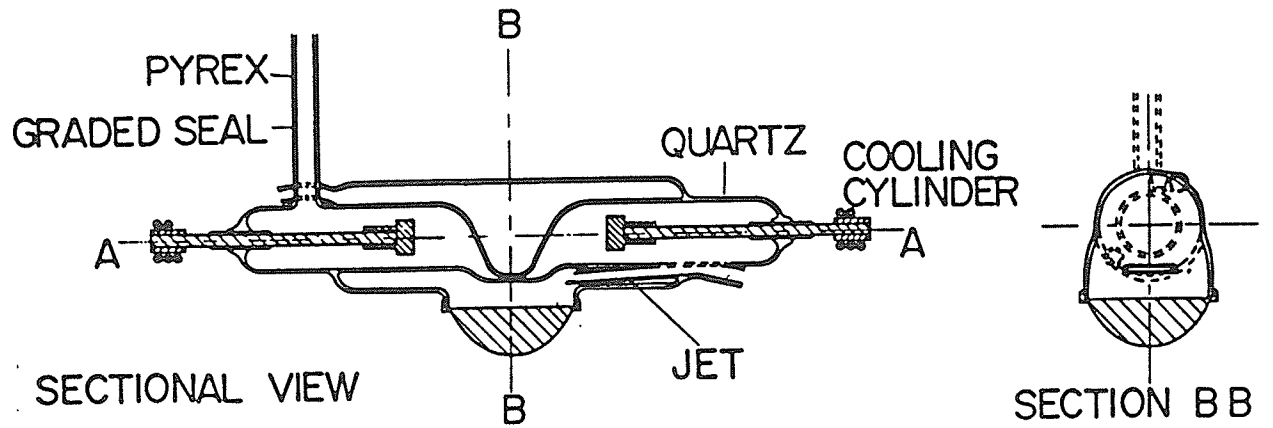
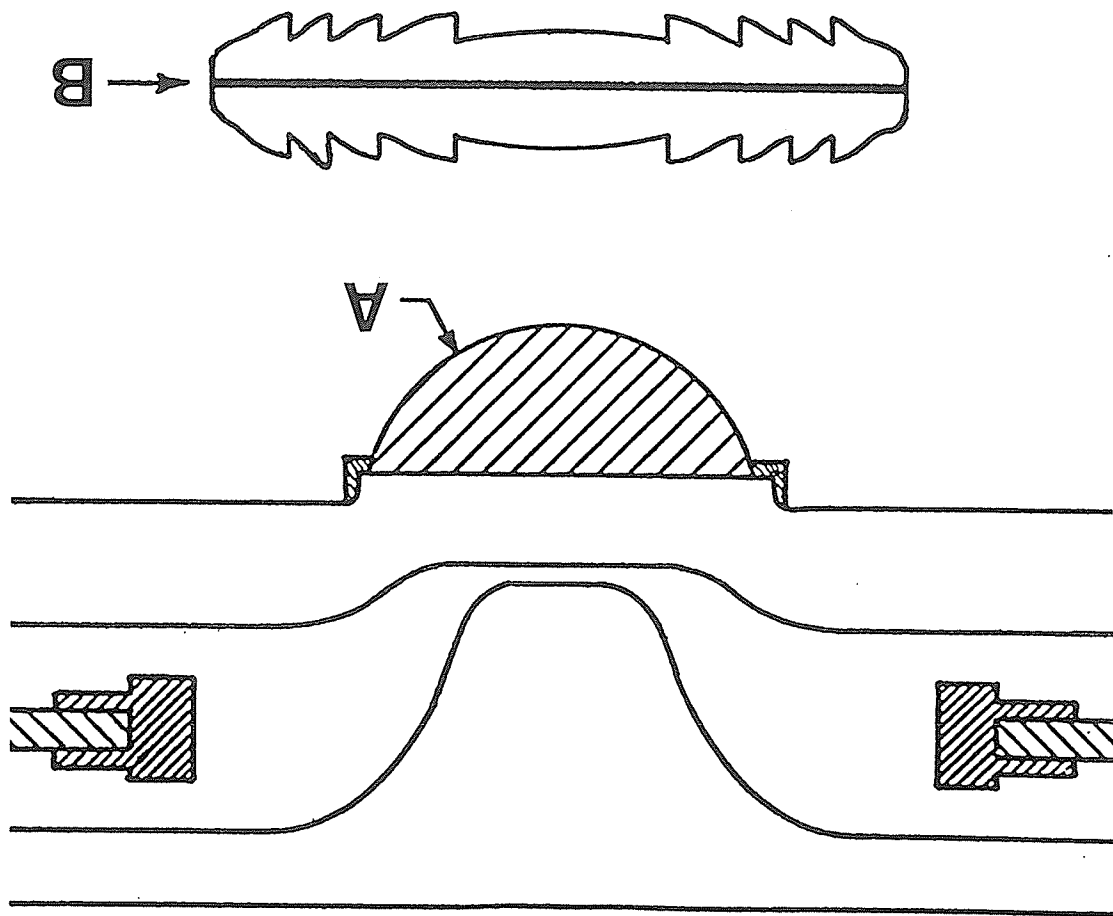


FIGURE 2.8 Details of the
pumping lamp and the polarizer, A=
Lucite lens, B= Polarizer cemented
between Fresnel lenses.



emitted by the lamp to be acceptable. The lamp was then kept connected to a station filled with pure Helium-4 at the appropriate pressure.

The pressure of the Helium-4 gas in the discharge tube was about 0.35 kPa (2.5 Torr). The gas was excited by a 600 Watt, 150 MHz R.F. power supply by the internal electrodes which can be matched to a 50 Ohm line, without reflections, using a pi network.

Each lamp is able to produce up to 1.4×10^{17} photons/sec at the 1.083 micrometers wavelength. After one week the power output of the lamp diminishes, due to impurities created by the sputtering. The decrease in output of the lamp can be reduced by tuning the lamp to higher power levels but only for a short period of time in order to prevent damage.

The polarizer is made of a pair of Fresnel lenses (76 mm diameter and 76 mm focal length), an infrared sheet type "HR" by Polaroid and a $\lambda/4$ wave plate, formed from two pieces of cellophane placed in series [Dan67]. The lenses, polaroid sheet and cellophane sheets were then glued together using epoxy, to reduce reflection losses.

iii) Magnetic field

The uniform magnetic field was produced by a pair of circular Helmholtz coils with equal numbers of turns and equal diameters, arranged with common axis. In this arrangement the distance between the two coils is equal to their radius (31 cm). The two coils were connected in series and were powered by a well regulated D.C. power supply. The variation of the field strength near the apparatus was minimal and the field was uniform at the center. The maximum field at the center of the coils was 4.2 mT (Figure 2.6).

The Helium-3 gas filled cell was placed at the geometrical center of the Helmholtz coils, which was the frame of the apparatus for the preliminary polarization measurements. Two electrode rings were placed on the Helium-3 cell which were connected to a 1 MHz R.F. power supply. A weak discharge was produced and 2^3S_1 metastable atoms were created. The light source was shielded in an aluminum box attached to the top coil.

To increase the total intensity (available photons) a second light source was attached to the bottom coil giving opposite circular polarization. Beckmann et al. [Bec77], used a mirror which reflected 20% of the incident light to increase the photons instead of a second lamp. Although in this way the polarization increases over that of a single lamp arrangement, measurements showed the increase is not as great as for two lamps. The cause was found in the fact that a

considerable amount of pumping light (about 30%) is already absorbed in the cell at the first passage and therefore the total light intensity is less than with two lamps.

E. POLARIZATION MEASUREMENTS

A reliable method of measuring the polarization produced in Helium-3 by optical pumping was essential to our work.

The technique used here measured the polarization P of the metastable 2^3S_1 levels and relied upon the theoretical equality of the polarization of the 2^3S_1 atoms to that of the ground state 1^1S_0 atoms to determine the polarization of Helium-3 gas.

The "traditional" method [Col63] for measuring polarization involves measuring the fraction of the pumping light which is absorbed. In this method the quantities $[I(0) - I(P)]$ and $I(0)$ are obtained in a sequence of measurements which involve depolarizing the Helium-3 target. From the ratio $[I(0) - I(P)]/I(0)$ the polarization can be calculated by applying equation (II.7). A brief description of the "traditional" method will be given in the next chapter.

Polarization of a particular cell takes an average of fifteen minutes before the desired fluorescence signal is reached. A full cycle of measurements includes observations of the fluorescence signal, S_f , destruction of the polarization, S_{12} , observation of the fluorescence signal after its destruction, S_{23} , and subtraction of the background (noise, stray light), S_{45} . The polarization calculation presupposes that the fluorescence signal from pumping

light absorption is proportional to that absorbed, thus the relative change in fluorescence is related to the polarization by:

$$\frac{S_{12}}{S_{23}-S_{45}} = \frac{S_f(O)-S_f(P)}{S_f(O)} = \frac{1}{\sum_{m=-1}^1 R_m (1-I_m(P))} \quad (II.8)$$

where S_{12}, S_{23}, S_{45} are the observed signals in arbitrary units, (with 1 to 5 the various stages in the measuring cycle in figure 3.9). S_f =fluorescence signal from pumping light, R_m = relative rates of $m=-1,0,+1$, transitions and $I_m(P)$ =photon absorption rate.

The fluorescence signal from the weak discharge, S_{45} , can be considered a correction to the above equation and also determines the discharge intensity. The optimum value for the weak discharge intensity was 0.65 ± 0.02 (in a scale from 0 to 1 mA). The latter can be used to demonstrate the dependence of polarization on the discharge intensity (Figure 2.9), through which an optimization for the polarization can be achieved.

Pumping light intensity measurements are obtained from the magnitude of the stray light reflected from the cell glass. The dependence of the polarization on the pumping light intensity is discussed in detail in Beckmann[Bec75]. The optimum value for the pumping light intensity was 0.53 ± 0.03 (in a scale of 0 to 5 volts). Beckmann et al.[Bec77], applies the differential equation for the

FIGURE 2.9 Weak discharge
intensity dependence of the
polarization.

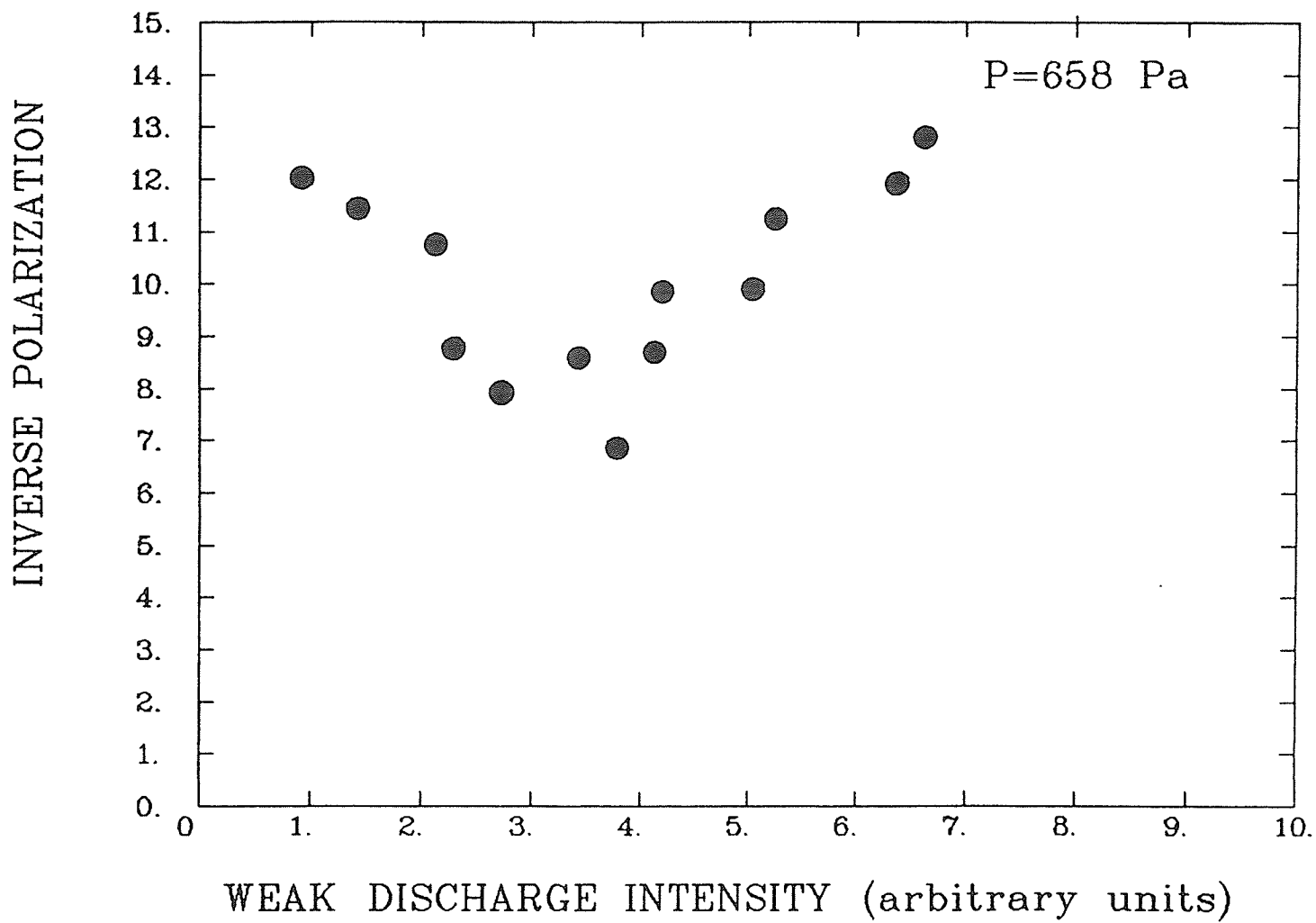


FIGURE 2.10 Pumping light
intensity dependence of the
polarization.

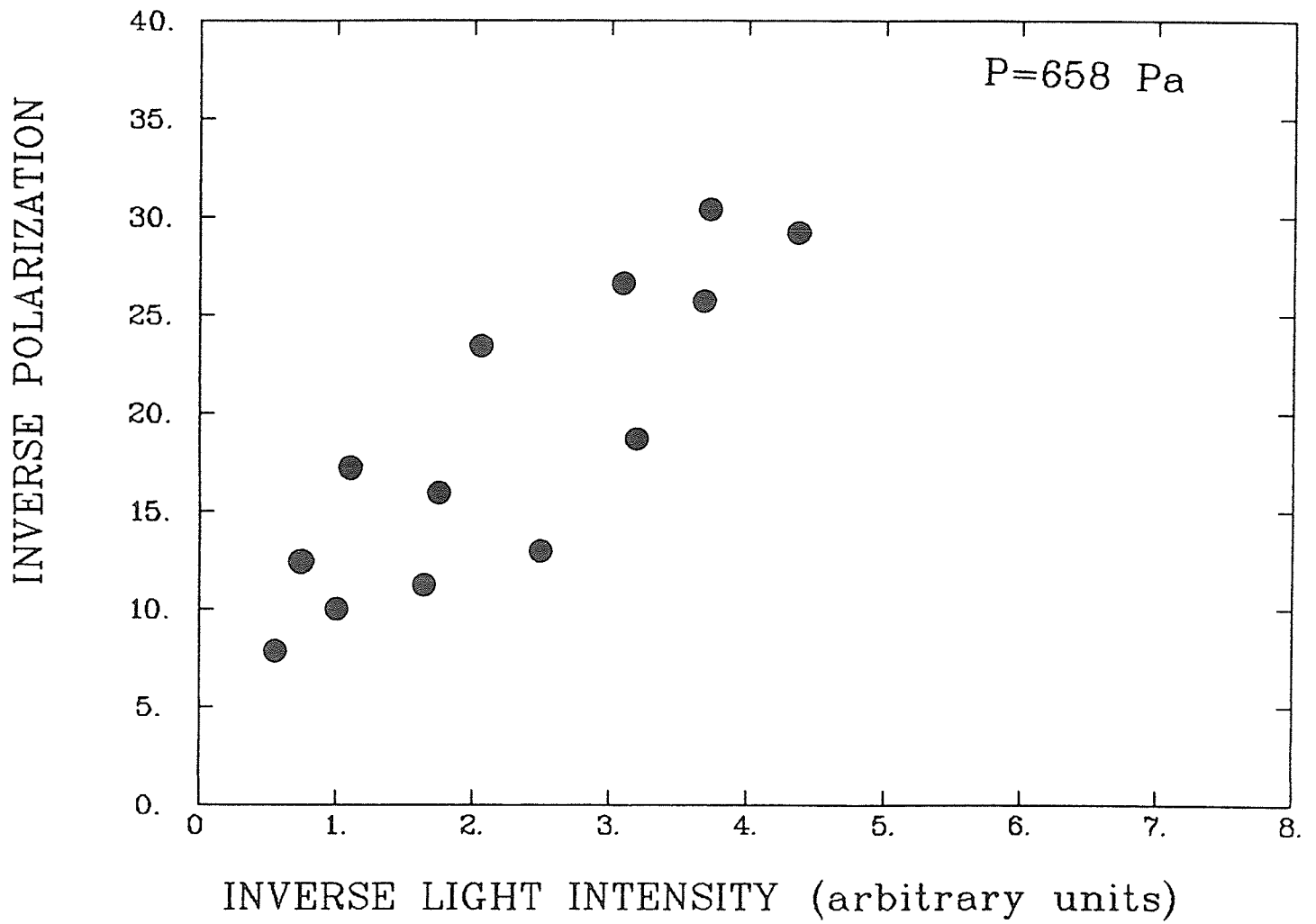
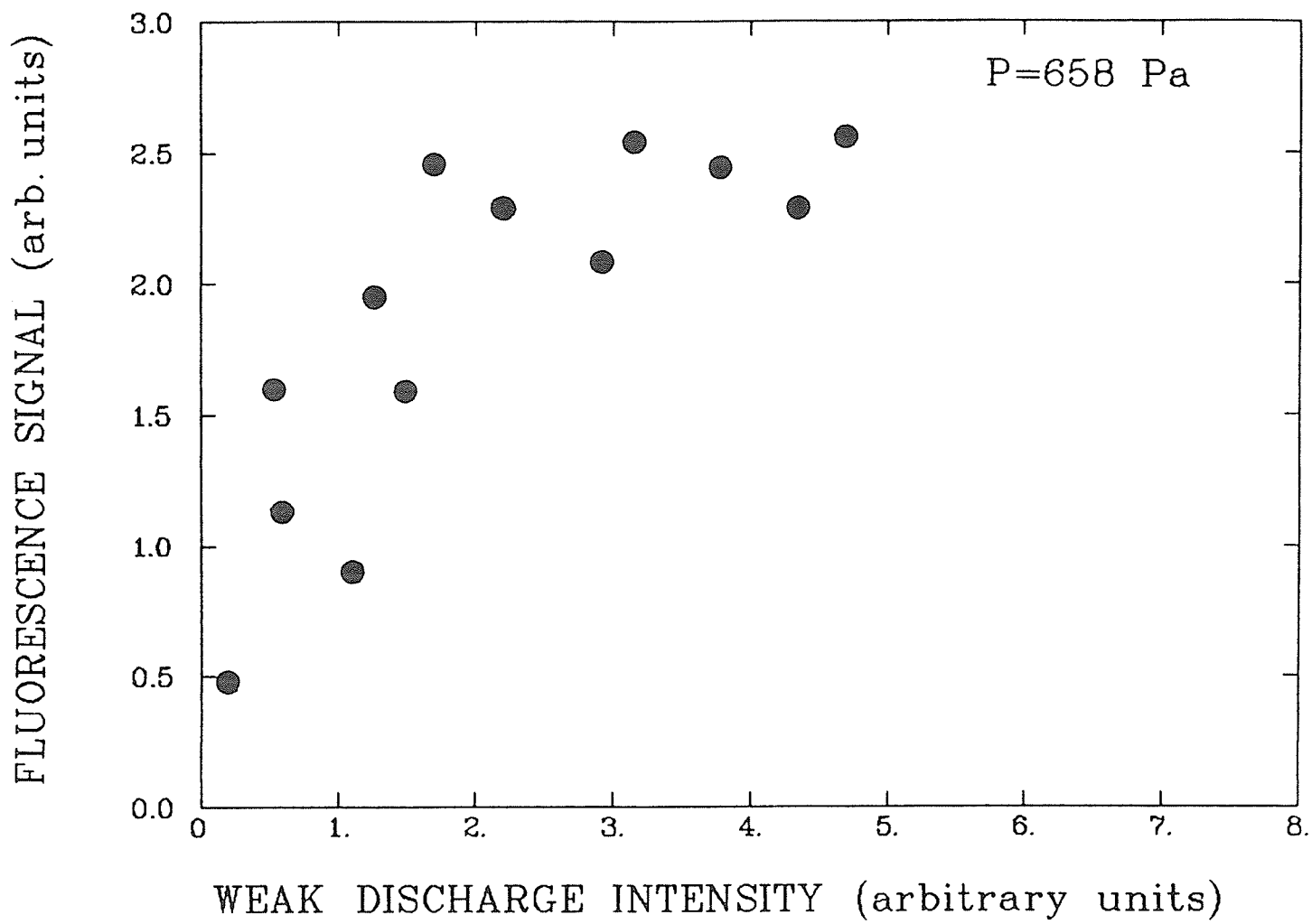


FIGURE 2.11 Fluorescence
signal as a function of the weak
discharge intensity.



nuclear polarization [Tim71b] and concludes that there must be a linear dependence between the reciprocals of the polarization and the pumping light intensity in the first approximation. This approximation is good for polarization values up to 30%. Figure 2.10 shows the above dependence for the study under discussion.

The polarization calculations assume that the fluorescence signal from the reemitted photons is proportional to the absorption rate per atom. Verheijen [Ver83] suggested a different formula to calculate the absorption rate per atom since the absorption factor can be estimated successfully from figure 2.10 and the targets are not always spherical. He also maintains that the equation confirms a non-linear relation between the fluorescence signal and the weak discharge intensity, especially in the high pressure cells. His approach seems to have a better accuracy due to the precise geometrical factor in the equation. Figure 2.11 shows the relation between the fluorescence signal and the weak discharge intensity in our work.

CHAPTER III

SCATTERING EXPERIMENT

A. INTRODUCTION

The aim of this chapter is to describe the facilities and equipment used in the measurement of the analyzing power for proton elastic scattering from polarized Helium-3.

The experiment was performed at the University of Manitoba Cyclotron Laboratory. Protons of 40.4 MeV were incident on a polarized Helium-3 target, which was developed for this experiment[Ver83]. The incident beam was under automatic computer control to ensure the stability of beam position at the target. The polarization was determined by an apparatus identical to that described in chapter two. The scattering chamber was designed for the experiment in order to incorporate the polarized target. The detection system consisted of detector telescopes placed at regular angular intervals around the target. For the data acquisition electronics interfaced to CAMAC was used and a data acquisition program was written especially for this experiment.

The following sections will describe the above in a more detailed and informative manner.

B. CYCLOTRON FACILITY

A duoplasmatron ion source was used to produce the unpolarized beam. The theory of operation and construction of this type of ion source is detailed in numerous articles (see, for example, Lejeune 1974).

The intention here is to outline the production of the beam used in the present study. The duoplasmatron is developed from a low pressure arc running between a cathode and an anode which is modified by an intermediate electrode and a magnetic field, concentrated near the anode. A double sheath exists in the plasma developed in the region of the intermediate electrode dividing the discharge into two parts, the cathode and the anode plasma. Electrons emitted from the cathode pass through the cathode plasma and are then accelerated across the double sheath. This beam is primarily responsible for the ionization and the arc forms around it. The ions are extracted through a small aperture in the anode. Electrons and ions are allowed to flow, due to high density, into an expansion cup where the density falls to acceptable values. The desired ion current is 1 mA and it can reach a maximum value of 20 mA. The gas pressure ranges from 20 Pa (0.15 Torr) to 106 Pa (0.8 Torr).

The University of Manitoba sector focused cyclotron was constructed in 1965 and it accelerates H^- ions to energies between 20 and 50 MeV. The axial injection system injects a beam of ions into the center of the cyclotron (Figure 3.1). The ions are deflected into the median plane by an electrostatic mirror and accelerated by a 28 kV R.F. voltage. Extraction is achieved by stripping the two electrons from the negative hydrogen ions using a thin aluminum foil. The magnetic force produced in the cyclotron reverses, sweeping the beam out of the cyclotron field. Changing the radius and angle at which the stripper foil is placed and use of a small magnetic field (the combination magnet), allows for extraction of proton beams having variable energy.

The layout of the cyclotron is shown in figure 3.2. The emerging proton beam is guided to the switching magnet through a series of quadrupoles and steering magnets. The switching magnet is used to bend the proton beam 30 degrees to the left into beamline B.

FIGURE 3.1 Duoplasmatron ion
source and injection system.

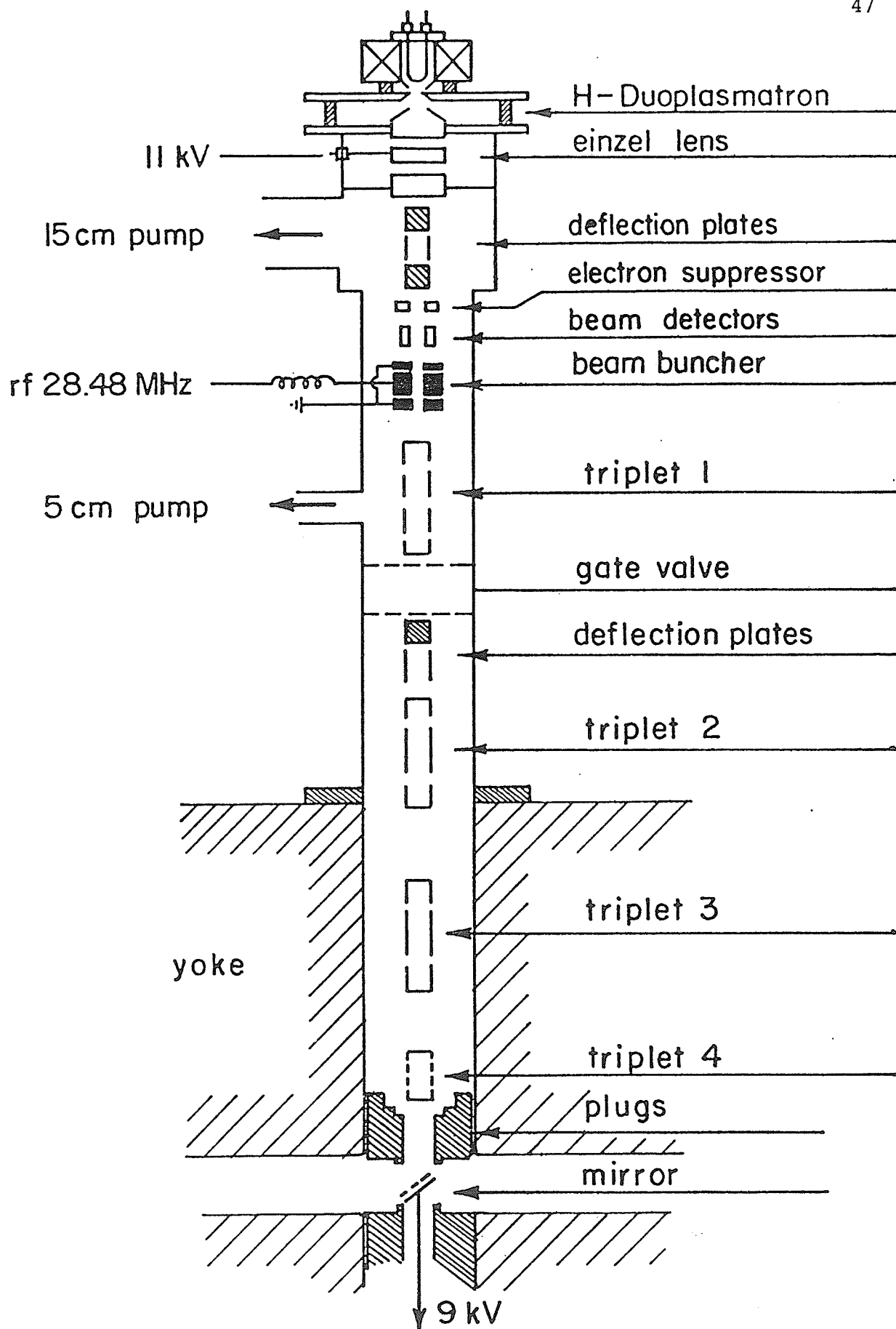
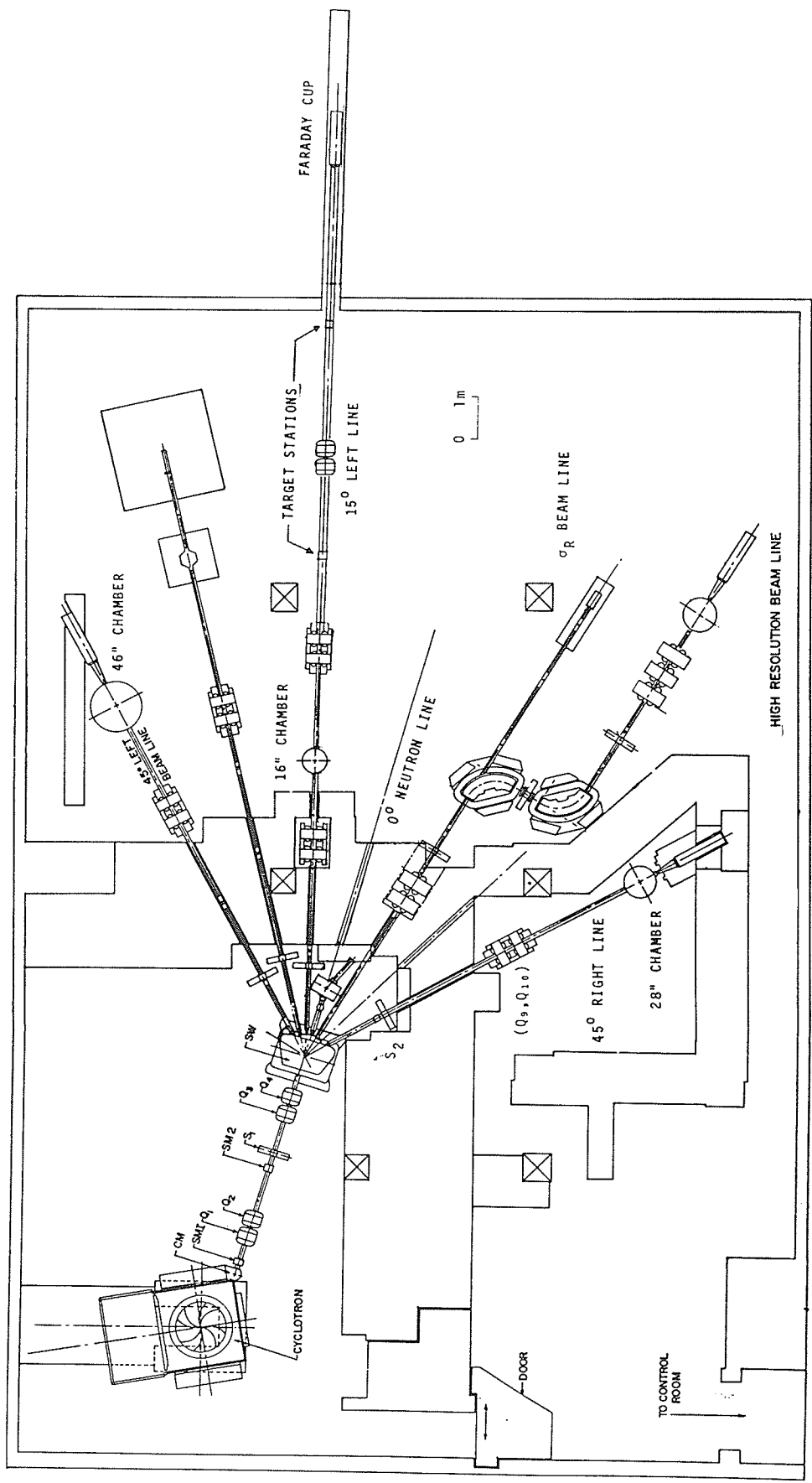


FIGURE 3.2 General
experimental area of the cyclotron
laboratory.



C. BEAM LINE

The polarized Helium-3 target is presently assembled on the 30 degrees left beam line (Figure 3.3).

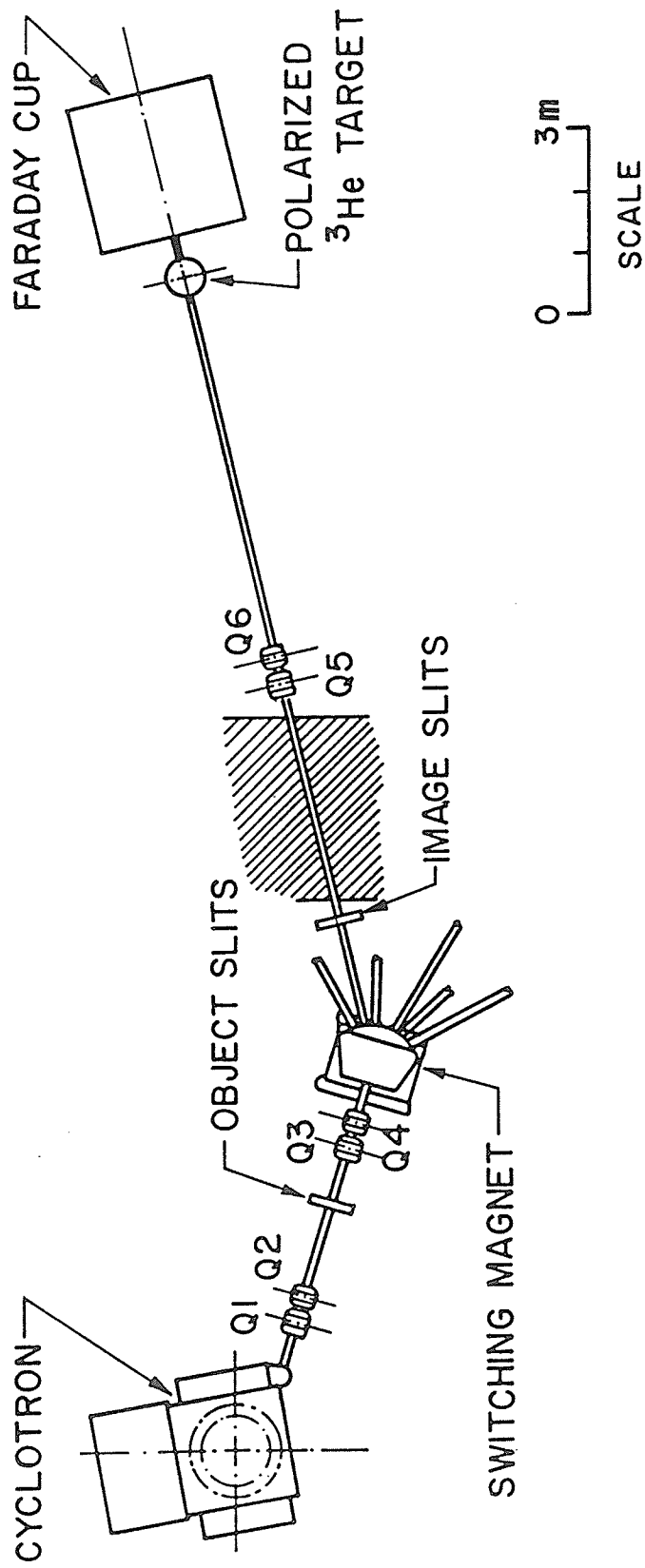
After leaving the cyclotron, the proton beam is guided through a quadrupole doublet Q1, Q2 onto a waist at the first set of slits. The quadrupole Q4 is used to give an energy focus, by reducing the focal length of the bending magnet, on the momentum defining set of slits.

The vertical and horizontal slits (object slits) define the object plane in front of the bending magnet. These slits are set at a separation of about 0.3 cm vertically and 0.2 cm horizontally. A second slit system (image slits) is placed at the focal plane of the bending magnet to momentum-analyze the proton beam used in the experiment. These slits have the same settings as the first set of slits. The slit setting corresponds to an energy spread of 200 KeV (FWHM) at 40.4 MeV. Screens S1, S2, S3 and S4 can be lowered into the beamline to monitor the beam transport by means of closed circuit television. Steering magnets ST1, ST2 and ST3 are available to center the beam with respect to the axis of the beamline. Beam transport calculations give the quadrupole magnet current $I(Q4)$ of:

$$I_{Q4} = \sqrt{E_p} (8.219 \pm 0.013) \quad (\text{III.1})$$

where E_p is the proton energy in MeV and $I(Q4)$ in amperes[Ver83].

FIGURE 3.3 Beamline B (30
degrees left) in experimental area
B.



The quadrupole magnet doublets QB5 and QB6 were used to focus the beam at the target position to a size of 4 mm width by 10 mm height, which was regularly inspected during the experiment by means of a screen inserted in front of the target position. Beam currents at the target were normally more than 100 nA and no more than 250 nA to limit count rates in the detectors.

Calibrations of the switching magnet were done by Verheijen[Ver83] using the cross-over technique. In this technique protons are inelastically scattered from carbon and elastically scattered from deuterium. The scattering angle at which these two peaks merge determines the proton beam energy and the zero degree axis of the scattering chamber. The protons were scattered from a CD₂ foil at various proton energies. At each energy the cross-over angle was determined for two excited states of ¹²C [Smy64]. The determination of the cross over angles and:

$$f = \frac{6.514 \sqrt{E_p (1876.5118 + E_p)}}{4.2577 \text{ G}} \quad (\text{III.2})$$

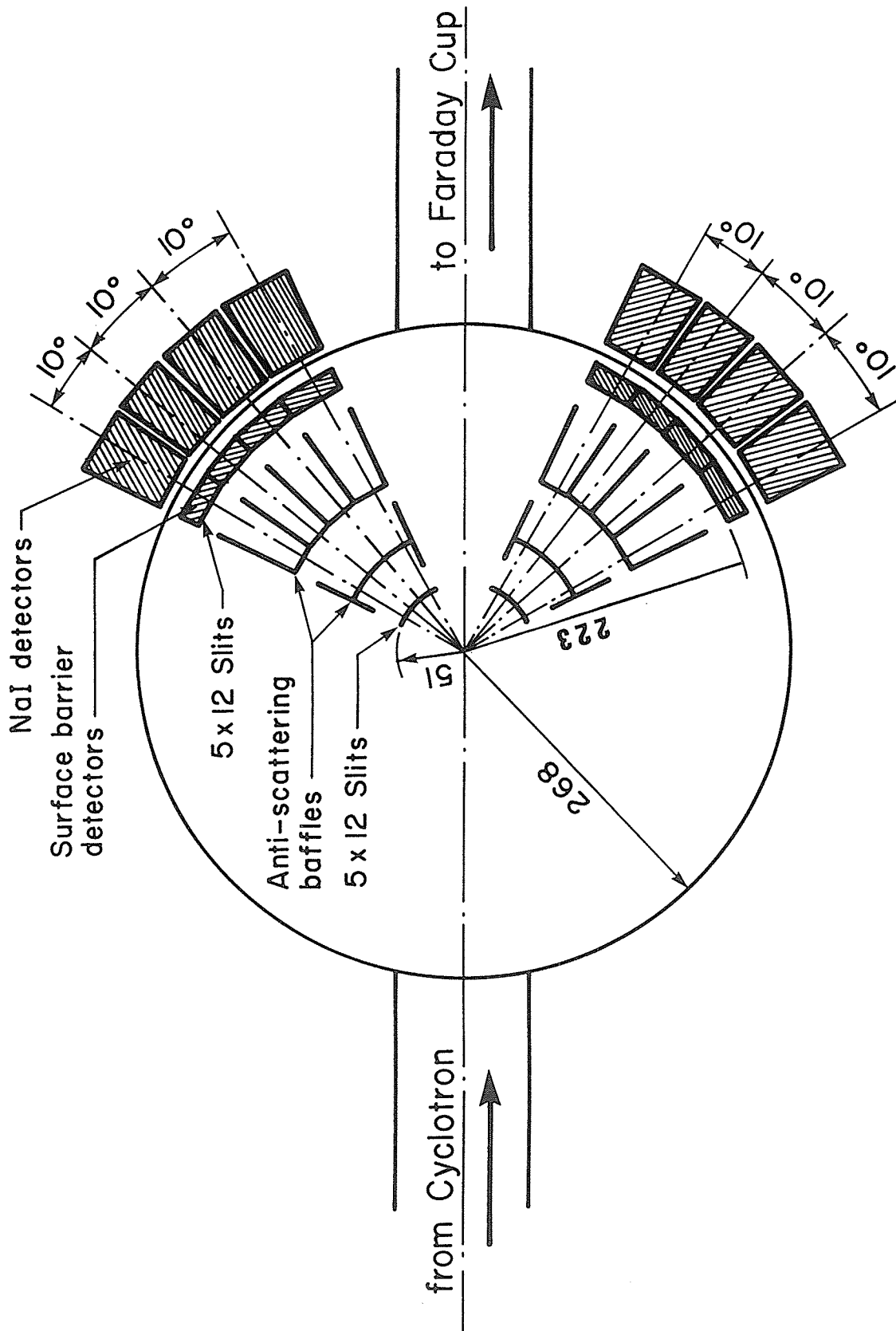
enabled calculation of the G-factor (constant). A measure for the field strength is the frequency, f in sec^{-1} (of the N.M.R. probe) which is measured as a function of the magnetic field (Gauss), and which is related to the kinetic energy T in MeV. In our study we used the value of $G=63.823(+/-0.12\%)$, and the energy was determined with an accuracy of $+/-0.24\%$.

D. SCATTERING CHAMBER

The aluminum scattering chamber used is about 45 cm in diameter and 12 cm high (Figure 3.4). Magnetic field gradients are minimized at the target by using non magnetic components. The interior of the chamber is machine finished and parts are coated with special black paint to minimize stray light on the target. The scattering chamber stand is bolted to the floor of the experimental area for rigidity. Two rotatable turntables are placed near the chamber, one in the top lid and the other in the bottom lid. Each turntable can be rotated from 0 to 180 degrees manually. The rotation is simultaneous for the inner and the outer part of each turntable through a gear. A digital readout of the position of each turntable in the chamber is provided by an external Decitrack shaft encoder. Before the beginning of the experiment the above system was carefully aligned.

Two sets of slits were mounted inside the chamber. The first was placed 51 mm from the geometrical center of the chamber, one on the top part and the other on the bottom part. In the present study we used slits of 3 mm thickness which are capable of stopping protons up to 45 MeV. These slits were made out of tantalum to reduce slit edge scattering. They had a width of 4.8 mm and a height of 12.7 mm. The solid angle defining slits at the rear were made of brass. They were used in conjunction with the surface barrier detectors. The slits were located 223 mm from the geometrical center of the chamber. The

FIGURE 3.4 Scattering chamber
(dimensions in mm).



angular resolution in polar angle Θ of the system was 2.0 degrees.

The chamber was designed to detect scattered protons in a range of angles from 15 degrees to 165 degrees. The windows on the Helium-3 cell were the limiting factor, so it was possible only to measure from 30 degrees to 150 degrees. The detection was made possible with a 19 mm wide window (slot) on the outer ring (cylindrical part) of the chamber covered with 0.13 mm thick kapton foil. This window covered an area from 10 degrees to 170 degrees, on both sides of the cylindrical part of the scattering chamber.

The beam of protons entered the scattering chamber, passed through the center of the chamber and came out through a 0.13 mm kapton foil. It then travelled through about 25 mm of air before entering the external Faraday cup through another kapton foil. The beam current was integrated using a current integrator for normalization purposes.

The target was placed at the geometrical center of the chamber in a special base made out of teflon, and aligned using an optical method. This method involved a light source, a mirror and a target mounted on a movable ladder.

Mounted on turntables in the scattering chamber were two arrays of detector telescopes ($\Delta E-E$). Each telescope consisted of a surface barrier detector (ΔE) and a sodium iodide detector (E) matched properly in gain. One array was mounted on the top turntable and the other on the bottom one. The surface barrier detectors in each array were placed in special detector holders made out of brass and were contained in the chamber vacuum. Each surface barrier detector consisted of the sensitive surface, which has evaporated on it a thin layer of gold, and the circular silicon wafer which is mounted on an insulating ring. The front surface of the ring is grounded to the housing of the detector. The back surface of the ring is connected to the center electrode of the connector which serves as the signal output and bias voltage connection (microdot).

The sodium iodide detectors were set behind the surface barrier detector outside the scattering chamber at a distance of a few centimeters. Each sodium iodide detector consisted of a single thallium-activated sodium iodide scintillation crystal NaI(Tl) (3.8 cm in diameter and 1.3 cm thick). The NaI(Tl) crystal was optically coupled to a photomultiplier tube (RCA 4523).

Two more sodium iodide detectors preceded by similar slit configurations were placed outside the scattering chamber. These two detectors served as monitors for the automatic beam location system. They were 20 degrees away from the axis of the beam, one to the left and the other to the right, near the Faraday cup. The output from the

two detectors was converted to a digital signal by the ADC (analog to digital converter) and fed to the computer. The computer stored the input in two regions, integrated the peaks (output of the detectors) and analyzed the results (stability ratio) through an acquisition program. The output of the computer was fed to a DAC (digital to analog converter) to activate the power supply in order to align the beam via a steering magnet when it was necessary. The steering magnet was mounted on the beam line, downstream from the Q5-Q6 quadrupole doublet (Figure 3.3). The power supply had a range of ± 1 volt and delivered ± 5 amperes.

E. NUCLEAR DATA COLLECTION

i) Electronics

The electronics configuration used in this experiment and a diagram for the relative timing of the pulses are shown in figures 3.5 and 3.6 respectively.

In the present study, at both forward angles (less than 90 degrees) and backward angles (greater than 90 degrees) telescopes were used since the scattered protons were energetic enough to pass the ΔE surface barrier detectors.

As noted in the previous section, the detection system consisted of silicon surface barrier (passing) detectors of 200 mm^2 area and 200 micrometers thickness inside the chamber and sodium iodide stopping detectors outside the chamber, comprising two arrays of ΔE -E particle telescopes. The telescopes were placed to the left and right of the direction of propagation of the beam. A set of two collimators was placed in front of each detector (Table 3.1).

Electrical connections to the surface barrier detectors were made by coaxial cables with vacuum feed-throughs in ports on the top and bottom lids of the chamber. The electrical connections for the sodium iodide detectors were made by coaxial cables as well as with regular feed-throughs in the end of each detector base. Before installing the

FIGURE 3.5 Electronics diagram
for one telescope. PA=
preamplifier, SA= spectroscopy
amplifier, TSCA= timing single
channel analyzer, HV= high voltage
supply, C= coincidence unit, LGS=
linear gate and pulse stretcher,
DSI= dual sum and inverter.

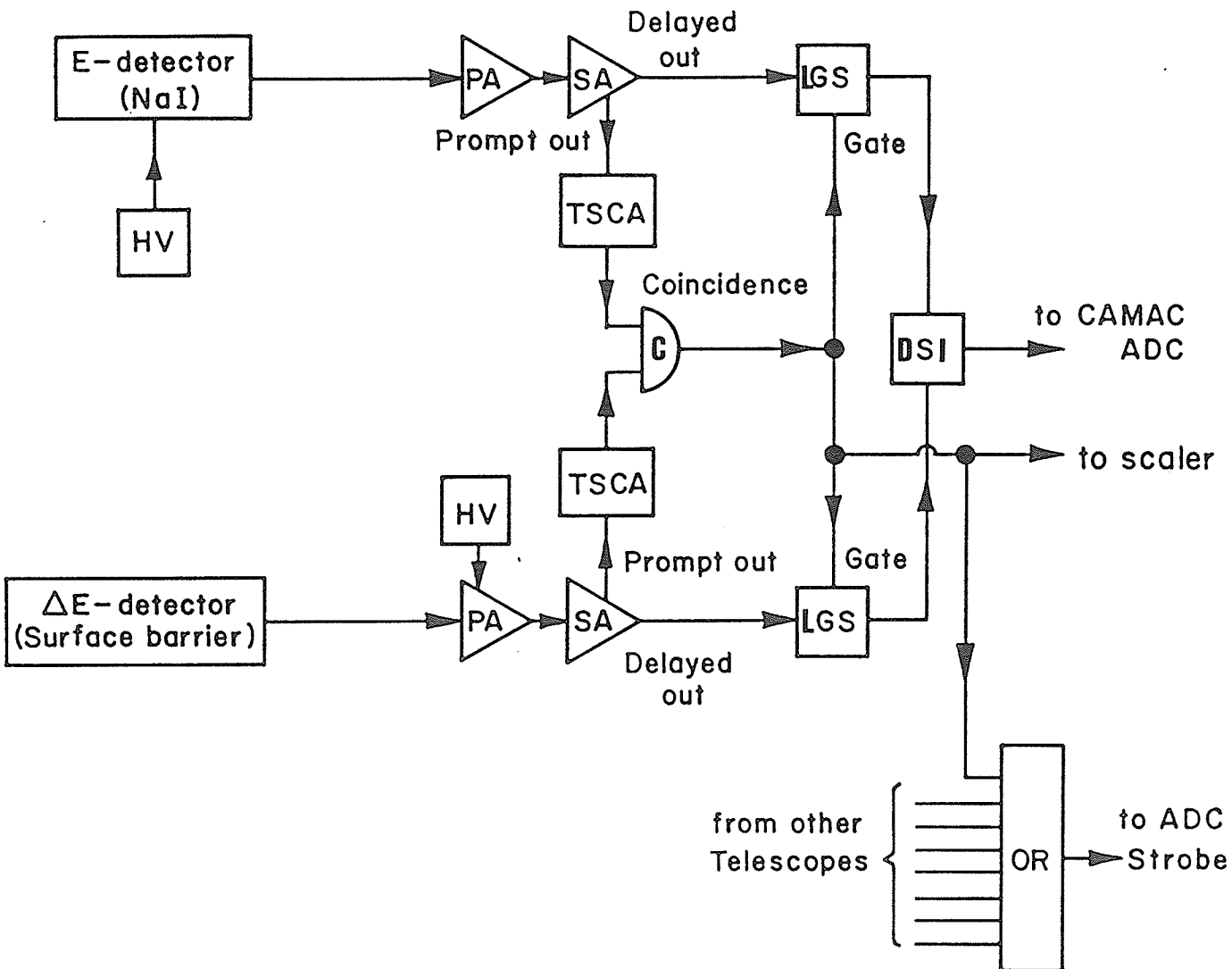
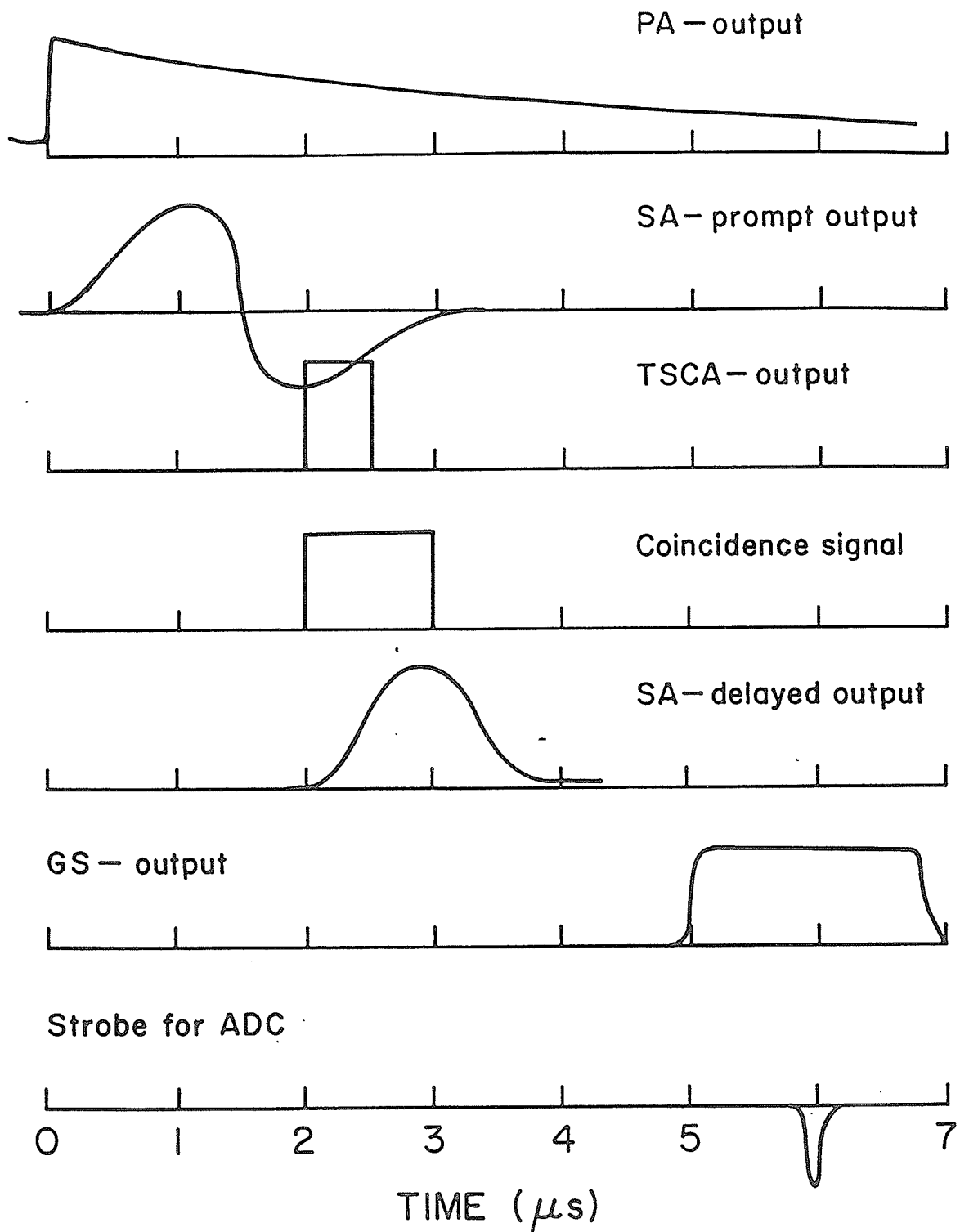


FIGURE 3.6 Timing diagram.



Angle		Front aperture width height (mm) (mm)	Rear aperture width height (mm) (mm)	Front-rear distance (mm)	Center-front distance (mm)
first	Left	4.764 12.736	5.795 12.698	171.02	50.121
	Right	4.726 12.622	5.672 12.691	171.05	50.378
+10	Left	4.711 12.647	4.759 12.691	170.93	50.446
	Right	4.725 12.686	4.791 12.676	170.98	50.369
+20	Left	4.721 12.673	4.757 12.727	170.81	50.256
	Right	4.751 12.665	4.792 12.701	170.93	50.424
+30	Left	4.752 12.679	5.741 12.712	170.88	50.147
	Right	4.713 12.714	5.494 12.693	170.93	50.372
Error:		$\pm 0.006 \pm 0.010$	$\pm 0.005 \pm 0.006$	± 0.05	± 0.004

TABLE 3.1 Aperture dimensions (in mm).

detectors, the sodium iodide detectors were tested for best resolution using a cobalt-60 source. Immediately outside the chamber the signals from the detectors were pre-amplified. Afterwards, the signals were carried by cables placed in a grounded metal cabinet conduit, to reduce background electrical noise, to the amplifiers in the control room. The two signals E and ΔE , from each telescope were then amplified and sent to TSCA's (timing signal channel analyzer), which were used to set thresholds and provide timing signals. The outputs of the TSCA's were sent to a coincidence unit, the output of which was used to gate the linear signals in the LGS (linear gate and stretcher), operated in "normally closed" mode. The linear signals entering the LGS units were the unipolar, delayed outputs of the spectroscopy amplifiers. The timing of the linear and logic signals was set as in figure 3.6. A pair of signals from the LGS's were added in the DSI (dual sum and inverter) amplifier and presented at the input of the ADC (analog to digital converter). The ADC started the signal conversion when a strobe pulse was supplied, which was derived from the logic signal representing a coincidence at a particular telescope. A VAX 11/750 computer registered the coincidence spectra from the eight telescopes.

ii) Dead Time Corrections

The dead time corrections were obtained by comparing the total number of counts in a coincidence spectrum with the actual numbers of coincidences presented to the ADC, separately recorded by a scaler for each telescope. An extensive discussion will be presented in chapter IV.

iii) Nuclear reactions in the detector material.

Some protons which are elastically scattered from the target into the detector are lost by undergoing nuclear reactions in the sodium iodide detector material. For each measurement, the energy of the elastically scattered protons entering the detector is calculated. The percentage loss due to nuclear reactions in the detector material was found by interpolation of the results of Sourkes et al.[Sou77] and was always less than 1.3% on the yields.

iv) Measurement Procedure

Before the actual runs were completed, a test of the background spectra was made. Trials with spherical cells showed that protons could be doubly scattered into the detectors, due to the slits, or from the cell wall at the entry point. The target cells (Figure 2.2) were designed with the extensions to reduce background as much as possible. Once a proton beam with the desired energy had been

obtained, the detector arrays were set at a specified angle and the experimental run started. These runs consisted of accumulating data in the form of spectra from the two detector arrays. The criteria for finishing a run was to obtain a certain number of counts, 370,000 for the smallest angle (40 degrees lab) and 16,000 for the largest angle (130 degrees lab) on each cycle, in the Helium-3 peak area of the spectra. At the end of a run the eight spectra were stored on magnetic tape for later analysis and the scaler values for the detectors and Faraday cup were recorded. The value of polarization was also measured and recorded.

The experiment cycle consisted of four runs: a) magnetic field up, polarization up, b) magnetic field up, polarization down, c) magnetic field down, polarization down, and d) magnetic field down, polarization up. The duration of each run was about two hours, and a total cycle, four runs, lasted about nine to ten hours. Time was required to measure the polarization after each run, to repolarize the target and to stabilize the proton beam on the target.

The above sequence of magnetic field and polarization was followed because, between runs a-b and c-d, only the polarization is affected so that the count rate at the same detector can be compared in two pairs of sequential runs, where only the nuclear asymmetry changes sign. All spectra were stored including the calculated left-right asymmetries with their errors. The errors were determined using a subroutine especially written and incorporated in the data acquisition program. A measurement at each angle was repeated several

times to achieve the desired accuracy in the analyzing power (+/-0.03).

v) Instrumental Asymmetries

Asymmetries are introduced when the geometry parameters differ for the left and the right detector respectively, or because the protons are traversing the magnetic field, which changes their direction. The asymmetries were calculated from the experimental results using the following:

$$\epsilon = \frac{Y_L - Y_R}{Y_L + Y_R} \quad (\text{III.3})$$

where Y_L and Y_R represent the left and right detector yields. Alternatively the yield was given as:

$$Y = Y_0 (1 \pm \epsilon_n) \quad (\text{III.4})$$

where the + (-) sign is for the left (right) detector and Y_0 is the yield for the unpolarized target. The yield of the target (first approximation only) was given by the following formula:

$$Y = \frac{n_b N A_r W_f}{h R_r} \frac{\sigma(\theta, \psi)}{\sin(\theta)} \quad (\text{III.5})$$

where: n_b = number of particles in the beam, N = target density (in m^{-3}), A_r = area of rear aperture (in m^2), W_f = width of front aperture (in m), h = distance between slits (thickness included, in

m), R_r = distance from the center to the rear aperture (in m), σ = differential cross section (in m^2), Θ = scattering angle, and ψ = azimuthal angle.

The instrumental asymmetries present in this study are mostly due to the apparatus and to the magnetic field (B_0). The instrumental asymmetry (ϵ_1) is mostly due to the geometry of the apparatus and can be traced to: a) differences in slit dimensions, b) differences in aperture distances, c) misalignment of the apertures, d) difference in rotation axis, e) beam positioning. The latter was minimized by the use of an automatic beam control system [Pet72]. Table 4.2 demonstrates the instrumental asymmetries calculated from the left and the right yields [Rad81].

The magnetic asymmetry (ϵ_m) is due to the fact that the magnetic field of the target changes the scattering angle by a small amount $\Delta\Theta$. This change can be estimated by knowing the momentum of the particle before and after scattering and the magnetic field configuration. The typical value of $\Delta\Theta$ is about a quarter of a degree at 40 MeV.

The nuclear asymmetry is very small (less than 0.3) due to the low polarization (less than 0.13). In order to separate this asymmetry from the others the runs were designed as described earlier in this chapter. The instrumental and magnetic asymmetries give a total asymmetry of approximately 0.3, which should be compared to the nuclear asymmetry. Ideally the nuclear asymmetry should be much

greater than the total of magnetic and instrumental asymmetries.

The observed asymmetry (III.3), consists of a combination of the above asymmetries, thus equation (III.4) can be extended to:

$$Y = Y_o (1 \pm \epsilon_i) (1 \pm \epsilon_m) (1 \pm \epsilon_n) \quad (\text{III.6})$$

where ϵ_i , ϵ_m , ϵ_n are the instrumental, magnetic and nuclear asymmetries respectively.

F. OPTICAL DATA COLLECTION

The polarization apparatus described in chapter two of this study was adapted to the beam line (Figure 3.7). The Helmholtz coils were placed parallel to the scattering chamber, which made it possible to change the direction of the magnetic field, without disrupting the operation of the power supply. The direction of the polarization was changed by interchanging the two polarizers from the light sources.

Before each run the Helium-3 gas cell had to be polarized, a procedure which required an average of 15 to 20 minutes. At the end of each run the polarization was measured and recorded by an IBM P.C. using a special electronics board (DVM). A program was especially written to cycle through the procedure to measure the polarization. The polarization of the cells decayed slowly with time due to irradiation of the glass (Figure 3.8).

A photodiode, which was shielded from stray light, and a light collecting lens system were placed at right angles to the pumping light beam going through the target. The output of the detector was amplified and fed into the electronic board of the IBM computer. A pair of coils fed by a 60 Hz power supply was placed near the Helium-3 cell to provide a large field gradient when depolarization was required. The sequence of the polarization measurements was as follows (Figure 3.9):

FIGURE 3.7 Online polarization
apparatus.

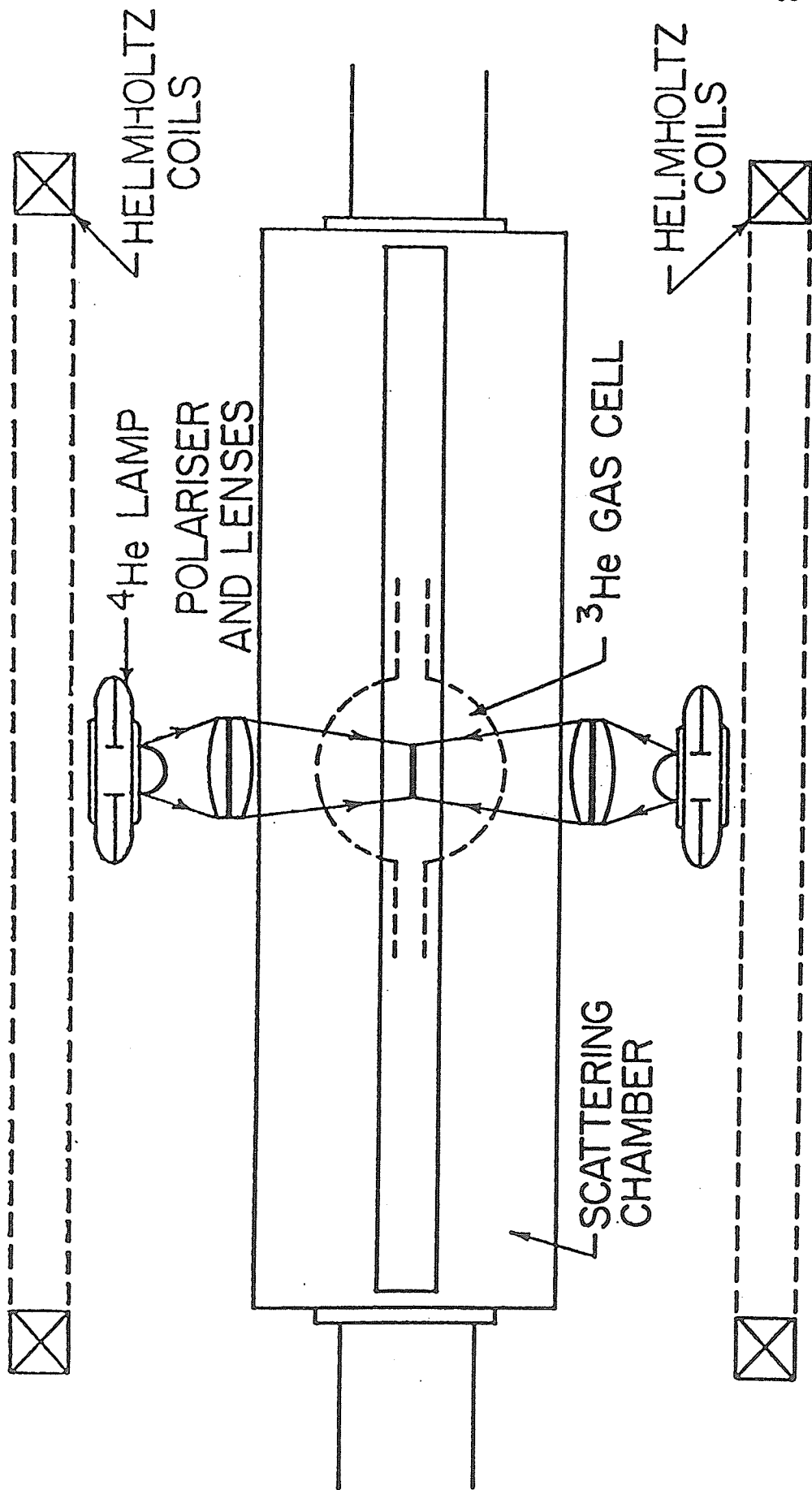
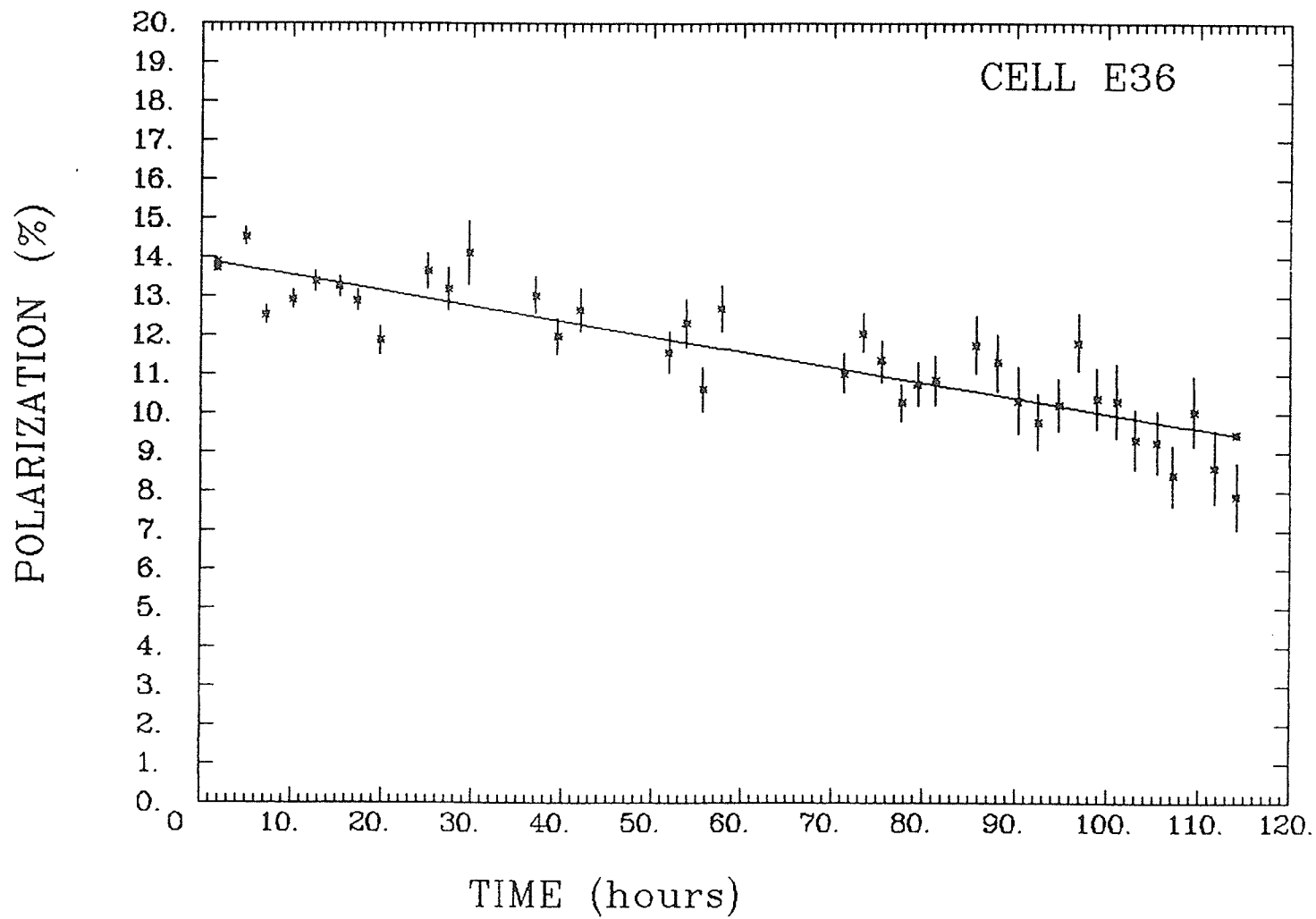


FIGURE 3.8 Polarization as a
function of time.



a) Measurement of the resonance radiation at right angles to the magnetic field when equilibrium polarization was reached. This gave the value of:

$$I(P) + I(SC) + I(WD) + G,$$

where $I(SC)$ is the intensity of the pumping light that reaches the photodetector through scattering from the cell, $I(WD)$ is the light intensity coming from the weak discharge, and G is the offset of the amplifier.

b) Depolarization of the atoms in the cell gives:

$$I(O) + I(SC) + I(WD) + G$$

c) Turning off the weak discharge gives:

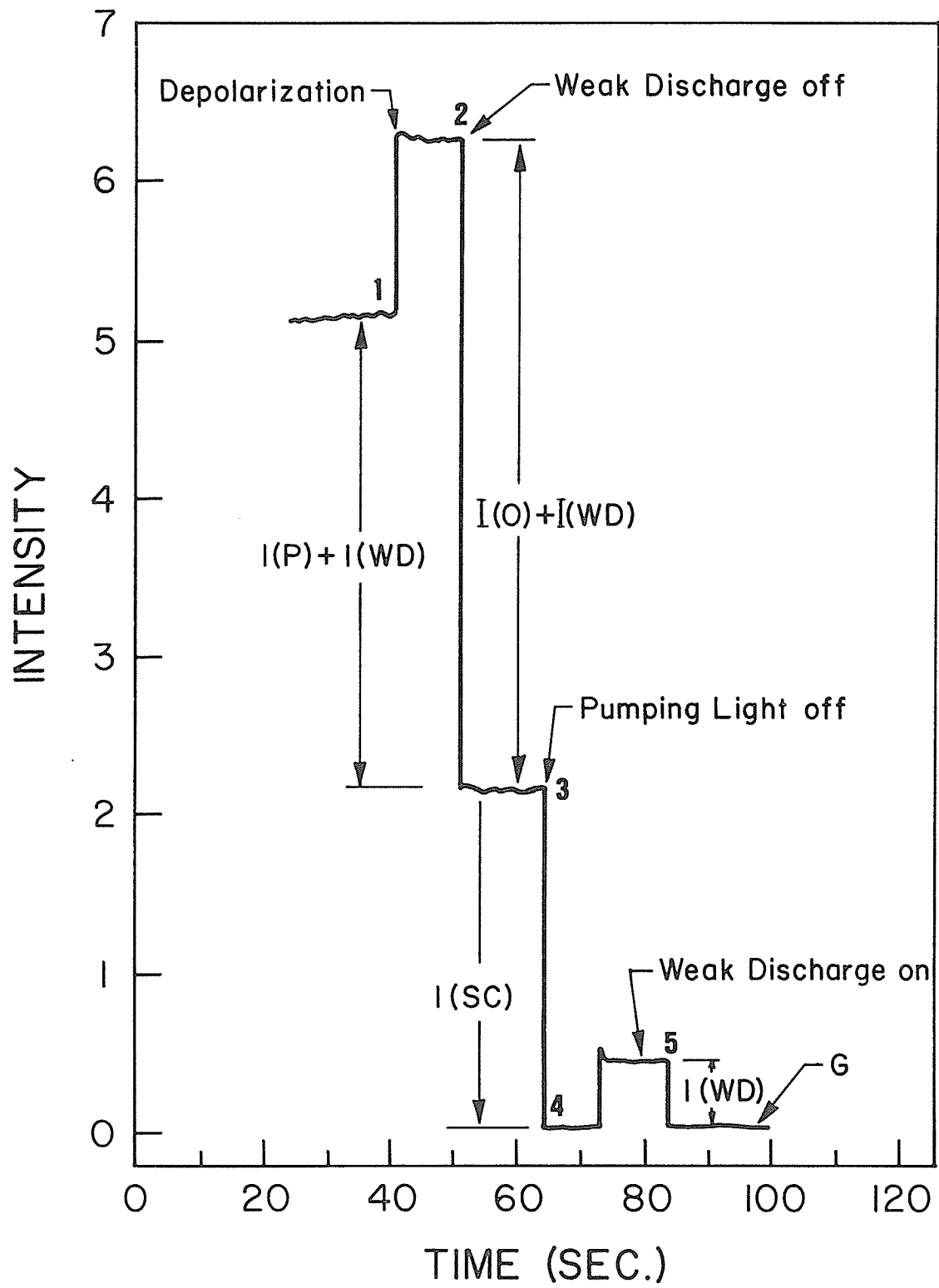
$$I(SC) + G$$

d) Turning off the pumping light and turning on the weak discharge gives: $I(WD) + G$

From the above measurements the ratio $[I(O) - I(P)] / I(O)$ can be calculated, and thus, by applying equation (II.7), the polarization.

The polarization measurements were also recorded on a chart graph recorder for verification. Two types of errors can be ascribed to the measurement of polarization, systematic errors and random errors. Systematic errors can originate from the uncertainty in the angle of detection. For the system under discussion this angle was 90 degrees.

FIGURE 3.9 Diagram of the
signals during a measurement cycle.



An optimization indicated that at smaller angles the uncertainty in the angle Θ is less significant. Random errors can originate from the fluctuation of the pumping light. The total error in P was of the order of ± 0.01 . This value was obtained by determining the polarization for a number of polarization-depolarization sequences and then calculating the standard deviation and the mean for the measured polarization.

CHAPTER IV

DATA ANALYSIS AND RESULTS

A. INTRODUCTION

The purpose of the data analysis completed in the present study was to determine the proton Helium-3 analyzing powers and false asymmetries. Scattering and polarization data for the reaction ${}^3\text{He}(p,p){}^3\text{He}$ were collected at 40.3 MeV between 40 degrees and 130 degrees in the laboratory. The collection procedure was discussed in chapter three of this study.

The data analysis can be separated into different stages:

- i) Peak area determination where the spectra are separated from the background.
- ii) Extraction of the analyzing powers, where the yields from the left and the right detectors are considered.
- iii) A set of checks that are necessary to assess the internal consistency of the data.

iv) Results and errors. This section will report the results after the first two stages of the analysis are completed, when the third stage indicates consistency of the results. An overview of possible errors will also be included.

B. PEAK AREA DETERMINATION

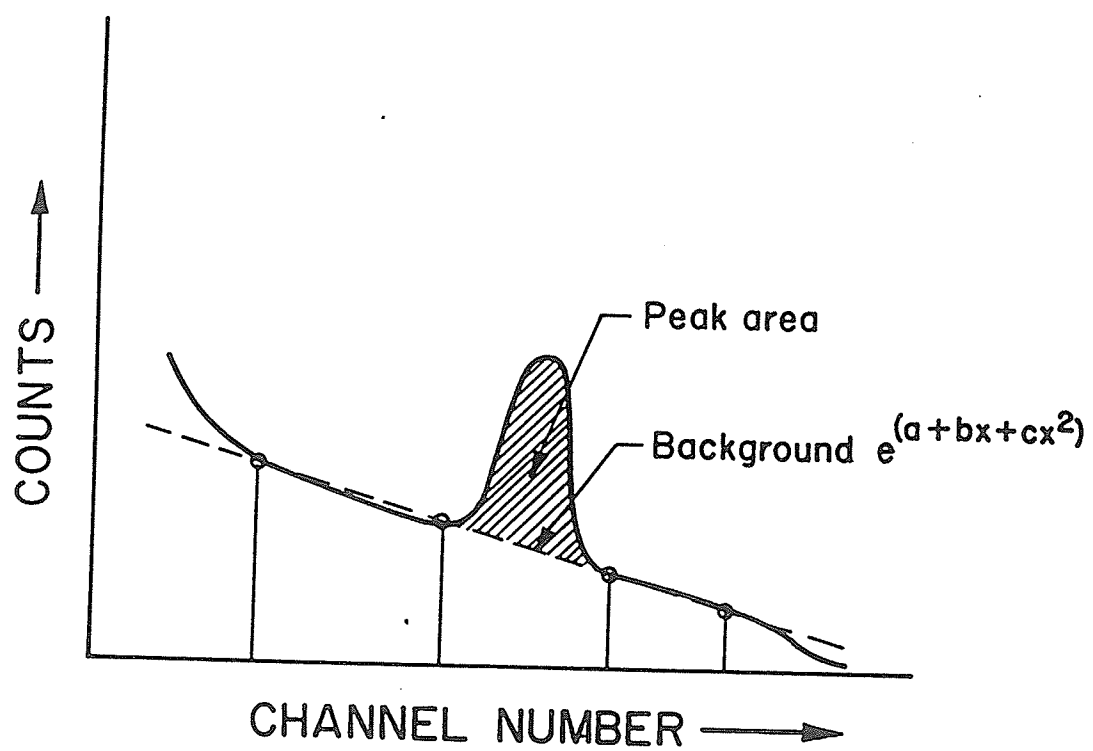
The spectra collected after each run were displayed on a screen in order to subtract the background. Normally, a simple background is determined on the basis of interpolation between two regions on either side of the elastic peak (Figure 4.1) using a function to approximate the shape of the background.

In the present study each spectrum was inspected individually. Two regions from each spectrum were selected for the determination of the background. The choice of regions required careful judgment, thus the procedure was repeated several times to minimize the error in the selection in order to improve the fit.

The form of the function for the background was in all cases a second order polynomial fitted to the logarithm of the channel counts. A second order polynomial proved in general to give the best fit to the background of all order polynomials used. Occasionally, a straight line fit to the logarithm of the channel counts gave a better chi-square fit.

A method used by Verheijen[Ver83] was to minimize the effect of systematic errors. This method requires the background to be fitted simultaneously to two spectra, taken with the same detector telescope in consecutive runs which had opposite target polarization but the

FIGURE 4.1 Illustration of the
method for defining the background
and determining the peak area.



same magnetic field. Using this method in our study, the systematic error did not improve as much as in Verheijen's case, therefore the single fit was used.

The peak areas were obtained by summation of all channel counts in the region between the two channels defining the peak and correcting this summation for the background (Figure 4.1). The statistical error was evaluated. Dead time corrections and NaI proton reaction losses were also applied. The dead time correction accounts for the fact that the yield obtained by integrating the elastic peak in the observed spectrum corresponds to events recorded by the computer and not the total numbers of protons scattered elastically.

When a pulse is processed by the computer, it is incapable of processing another pulse for a period of time τ after the first pulse. If R is the mean rate of pulses at the input, then let R' be the mean rate at the output where, of course $R > R'$. Since R' is the rate at which pulses are processed by the computer, it follows that in unit time the computer is 'dead' for a total time of $R'\tau$. The number of incident pulses occurring in that time is, on average $RR'\tau$ and all these are lost due to the dead time, $R - R' = RR'\tau$. This correction is less than 3% for the forward and backward angles.

C. ANALYZING POWER

The determination of the analyzing power, A_y , is dependent on the measurement of a nuclear scattering asymmetry, ϵ_n , (discussed in the previous chapter) and the polarization, P , of the target. These quantities are related by:

$$\epsilon_n = PA_y \quad (\text{VI.1})$$

The analyzing power, A_y , has also been referred to as an asymmetry, but in view of the Madison convention, this usage is discouraged.

At all four angles measured in a cycle, a total of eight peak areas at each angle were obtained from the four runs as described in chapter III.E. Szaloky et al.[Sza75] and Verheijen[Ver83] used a formalism to describe the yields in each of the eight peak areas. These yields are tabulated in table 4.1. The related asymmetries are described in terms of those yields. The magnetic asymmetry which is given in terms of an angle deviation $\Delta\Theta$, and the instrumental asymmetry[Sil59] which is included in the use of different geometry factors G and angles Θ for the left and right detectors are also included in the yields. The scattering cross sections used are noted by σ , the target density by N and n is the number of incident protons.

Run	spin	magn. field	yield
Left detector			
a	up	up	$Y_1 = n_a N G_L(\theta_L + \Delta\theta) \sigma(\theta_L + \Delta\theta) (1 + P_a A_y(\theta_L + \Delta\theta))$
b	down	up	$Y_2 = n_b N G_L(\theta_L + \Delta\theta) \sigma(\theta_L + \Delta\theta) (1 - P_b A_y(\theta_L + \Delta\theta))$
c	down	down	$Y_3 = n_c N G_L(\theta_L - \Delta\theta) \sigma(\theta_L - \Delta\theta) (1 - P_c A_y(\theta_L - \Delta\theta))$
d	up	down	$Y_4 = n_d N G_L(\theta_L - \Delta\theta) \sigma(\theta_L - \Delta\theta) (1 + P_d A_y(\theta_L - \Delta\theta))$
Right detector			
a	up	up	$Y_5 = n_a N G_R(\theta_R - \Delta\theta) \sigma(\theta_R - \Delta\theta) (1 - P_a A_y(\theta_R - \Delta\theta))$
b	down	up	$Y_6 = n_b N G_R(\theta_R - \Delta\theta) \sigma(\theta_R - \Delta\theta) (1 + P_b A_y(\theta_R - \Delta\theta))$
c	down	down	$Y_7 = n_c N G_R(\theta_R + \Delta\theta) \sigma(\theta_R + \Delta\theta) (1 + P_c A_y(\theta_R + \Delta\theta))$
d	up	down	$Y_8 = n_d N G_R(\theta_R + \Delta\theta) \sigma(\theta_R + \Delta\theta) (1 - P_d A_y(\theta_R + \Delta\theta))$

TABLE 4.1 Definitions of formulae for the determination of the nuclear scattering asymmetries.

Taking the yields from pairs of consecutive runs in table 4.1, using the same detector, and making sure that the magnetic field is the same, four estimates of the analyzing power are found.

$$A_y(\Theta_L + \Delta\theta) = \frac{Y_1/n_a - Y_2/n_b}{P_b Y_1/n_a + P_a Y_2/n_b} \quad (\text{VI.2})$$

and

$$A_y(\Theta_L - \Delta\theta) = \frac{Y_4/n_d - Y_3/n_c}{P_c Y_4/n_d + P_d Y_3/n_c} \quad (\text{VI.3})$$

and

$$A_y(\Theta_R - \Delta\theta) = \frac{Y_6/n_b - Y_5/n_a}{P_a Y_6/n_b + P_b Y_5/n_a} \quad (\text{VI.4})$$

and

$$A_y(\Theta_R + \Delta\theta) = \frac{Y_7/n_c - Y_8/n_d}{P_d Y_7/n_c + P_c Y_8/n_d} \quad (\text{VI.5})$$

Taking the averages of equation (IV.2) and (IV.3), and that of (IV.4) and (IV.5) gives two estimates in which the effects of the magnetic field asymmetry are eliminated up to the second order. The analyzing powers are also given at angles Θ_L and Θ_R :

$$A_y(\Theta_L) = [A_y(\Theta_L + \Delta\theta) + A_y(\Theta_L - \Delta\theta)] / 2 \pm \sigma_L \quad (\text{VI.6})$$

and

$$A_y(\Theta_R) = [A_y(\Theta_R + \Delta\theta) + A_y(\Theta_R - \Delta\theta)] / 2 \pm \sigma_R \quad (\text{VI.7})$$

where σ_L and σ_R are the errors as derived from the uncertainty in the yields.

Finally, taking a weighted average of equations (IV.6) and (IV.7) we obtain:

$$A_y(\Theta) = [A_y(\Theta_L)/\sigma_L^2 + A_y(\Theta_R)/\sigma_R^2] / (\frac{1}{\sigma_L^2} + \frac{1}{\sigma_R^2}) \quad (\text{VI.8})$$

A weighted average has to be considered in the last equation because there is a possibility that the errors in the peak areas are different for the left and right detectors. The total error in A_y can be evaluated using the errors in the uncertainties in the yields, the error in the polarization, the magnetic field asymmetry, and errors in Θ_L and Θ_R which even though they are very small, need to be taken into consideration.

A correction for the polarization was included by multiplying all analyzing powers by the factor 1.04. This factor describes the effect of a non ideal light source[Ver84] and is in accord with the kinematics of polarization described by Daniels et al.[Dan71a]. In our case the factor was an average since the data reported here were taken with three different cells.

D. INSTRUMENTAL AND MAGNETIC ASYMMETRIES

Having already calculated the polarization in each run and the analyzing power, we can easily estimate the instrumental (ϵ_i) and the magnetic (ϵ_m) asymmetries. Using equation (III.6) in the form of:

$$Y' \equiv \frac{Y}{nN(1 \pm PA_y)} = G_o(1 \pm \epsilon_i)(1 \pm \epsilon_m) \quad (\text{VI.9})$$

and taking the average of each pair from table 4.1

$$Y'_{12} = (Y'_1 + Y'_2)/2 = G_o(1 + \epsilon_i)(1 + \epsilon_m) \quad (\text{VI.10})$$

and

$$Y'_{34} = (Y'_3 + Y'_4)/2 = G_o(1 + \epsilon_i)(1 - \epsilon_m) \quad (\text{VI.11})$$

and

$$Y'_{56} = (Y'_5 + Y'_6)/2 = G_o(1 - \epsilon_i)(1 - \epsilon_m) \quad (\text{VI.12})$$

and

$$Y'_{78} = (Y'_7 + Y'_8)/2 = G_o(1 - \epsilon_i)(1 + \epsilon_m) \quad (\text{VI.13})$$

the instrumental and the magnetic asymmetries can be calculated from equations (IV.10) to (IV.13).

According to Verheijen[Ver83] the instrumental asymmetry will be (Table 4.2):

$$\epsilon_i = \frac{Y'_{12} + Y'_{34} - Y'_{56} - Y'_{78}}{Y'_{12} + Y'_{34} + Y'_{56} + Y'_{78}} \quad (\text{VI.14})$$

and the magnetic asymmetry will be (Table 4.2):

$$\epsilon_m = \frac{Y'_{12} - Y'_{34} - Y'_{56} + Y'_{78}}{Y'_{12} + Y'_{34} + Y'_{56} + Y'_{78}} \quad (\text{VI.15})$$

The instrumental asymmetry is related to the aperture dimensions of the detector and possible misalignment of the beam. The magnetic asymmetry is related to the effect of the magnetic field at the target (angle deviation). Both asymmetries can be verified if they remain constant at the same angle in consecutive cycles.

E. CONSISTENCY CHECKS

The consistency of the measurements for each cycle has been tested by evaluating the constant K (consistency factor)[Bak69;Ver83]:

$$K = \frac{r^{\frac{1}{2}} - 1}{r^{\frac{1}{2}} + 1} \quad (\text{VI.16})$$

where

$$r = \frac{Y_1 Y_3 Y_6 Y_8}{Y_2 Y_4 Y_5 Y_7} \quad (\text{VI.17})$$

and Y_i where $i=1,2,\dots,8$ represents the yields of the detectors.

The aim is to evaluate K and its error ΔK , and in order to reject a cycle, K has to be three times more than its error at the backward angles. An exception was made for forward angles where the errors due to counting statistics were small[Sza78b].

The constant K can have the value zero when the polarization is constant during all four runs ($P_a = P_b = P_c = P_d$)[Sza75].

Verheijen[Ver83] defines the use of K when all detector and magnetic field dependence is eliminated, up to the first order in the polarization. Therefore, K_p is considered a measure for the consistency of the polarization during a cycle and can be defined by:

$$K_p = [K - (P_a + P_b - P_c - P_d) A_y/4] / \Delta K \quad (\text{VI.18})$$

which should have approximately a normal distribution.

Rad et al.[Rad81] developed a method which compared the analyzing powers obtained from the left and right detectors by evaluating their difference in terms of their error. Therefore K_i is considered as a measure for the instrumental asymmetry and is defined by:

$$K_i = \frac{A_y(\theta_L) - A_y(\theta_R)}{\sqrt{\sigma_L^2 + \sigma_R^2}} \quad (\text{VI.19})$$

This equation is derived from equations (IV.6) and (IV.7), and is sensitive to any effects of the instrumental asymmetries in the analyzing power.

Similarly, a method was developed which compared the difference in the analyzing power obtained from the runs with magnetic field up and magnetic field down. Therefore K_m is considered as a measure for the magnetic asymmetry and is defined by:

$$K_m = \frac{A_y(+)-A_y(-)}{\sqrt{\sigma_+^2 + \sigma_-^2}} \quad (\text{VI.20})$$

where $A_y(+)$ is derived from the weighted average of equations (IV.2) and (IV.4) and $A_y(-)$ is derived from equations (IV.3) and (IV.5), which measure the influence of the magnetic field variation on the analyzing power[Rad81].

Finally, the overall fit of the equation:

$$Y = nNG_o(1 \pm \epsilon_i)(1 \pm \epsilon_m)(1 \pm PA_y) \quad (\text{VI.21})$$

to the data was tested by evaluating the sum of the squares:

$$\chi_Y^2 = \sum_{i=1}^8 \left(\frac{Y_{\text{exp},i} - Y_{\text{cal},i}}{\Delta Y_{\text{exp},i}} \right)^2 \quad (\text{VI.22})$$

where Y_{exp} and Y_{cal} are the experimental and the calculated yields respectively. A smooth curve is expected for chi-squared, if the distribution of deviations between the yields is a normal distribution with four degrees of freedom (Figure 4.2).

In several cases where some of the criteria were not met, a specific malfunctioning during the experiment could be traced, such as detector breakdown or decrease in target polarization. Such measurements were rejected. With these modifications the final analyzing powers were compiled. The distributions of K^2 were plotted as obtained from the analysis of the experimental data. The reduced chi-square was added also from equation(VI.22). The four histograms should have a chi-square distribution with one degree of freedom for K_m^2 (Figure 4.3) and two degrees of freedom for both K_i^2 (Figure 4.4) and K_p^2 (Figure 4.5) respectively. The histograms compare well with the ones from the study of Verheijen[Ver83]. The quality of the results could be judged from the consistency checks.

FIGURE 4.2 The distribution of
chi-square.

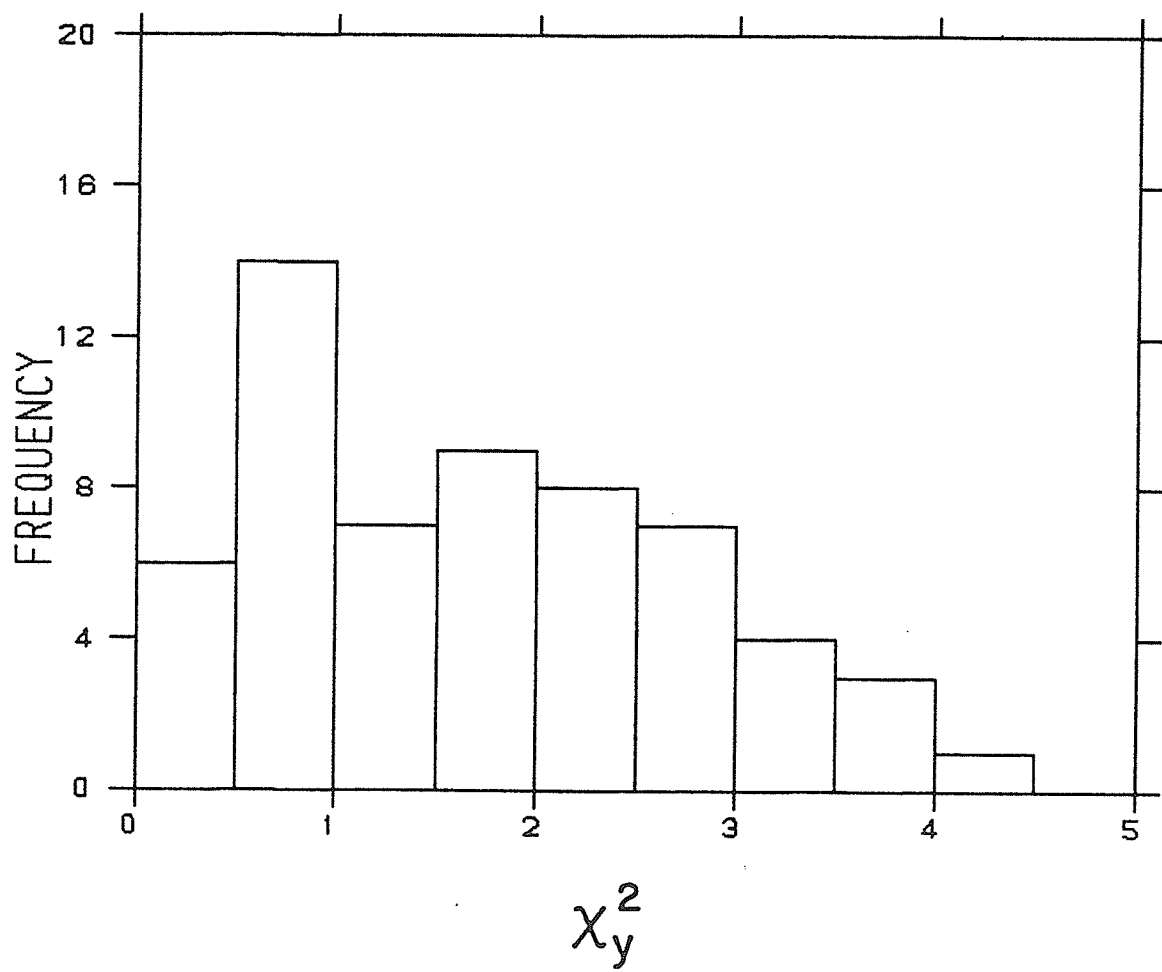


FIGURE 4.3 The distribution of
consistency checks for K_m^2 .

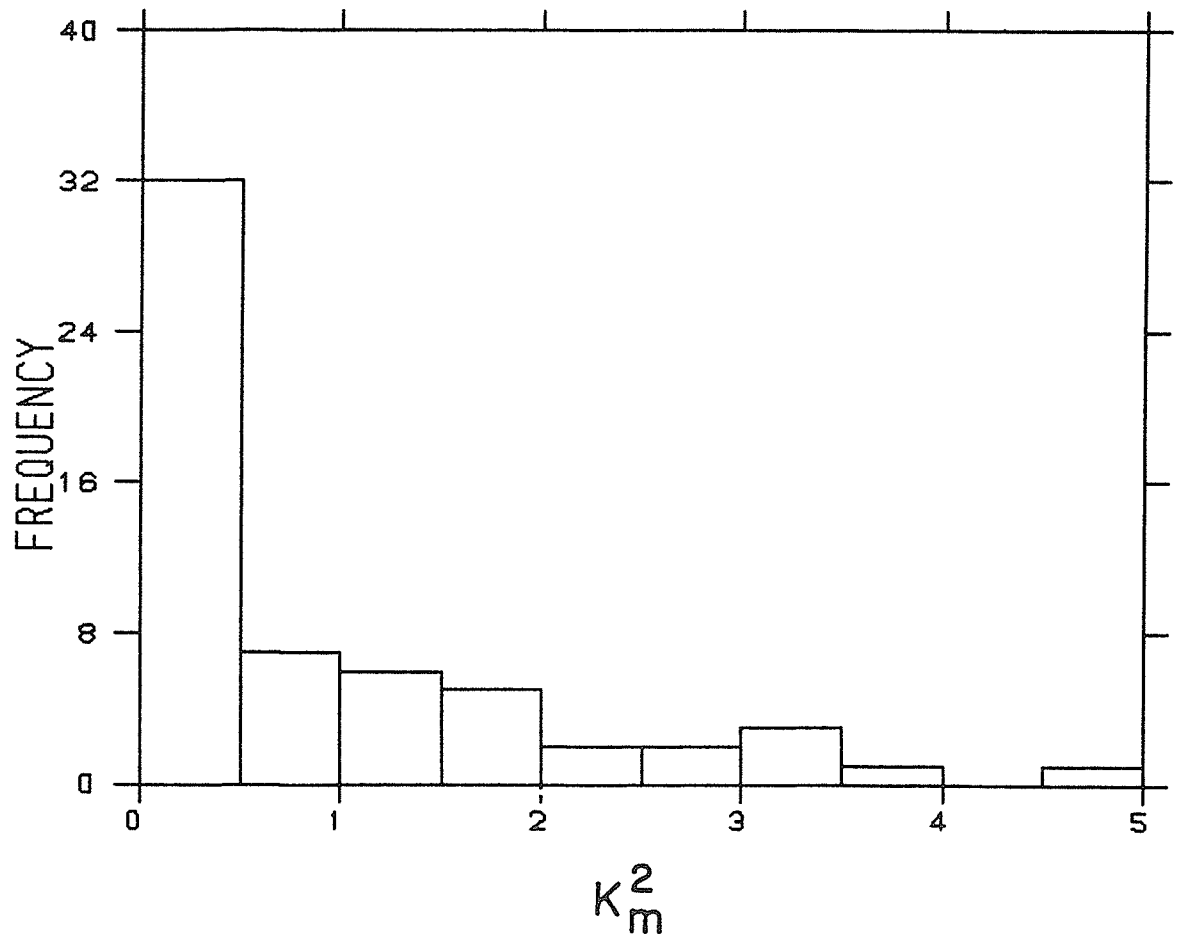


FIGURE 4.4 The distribution of
consistency checks for K_i^2 .

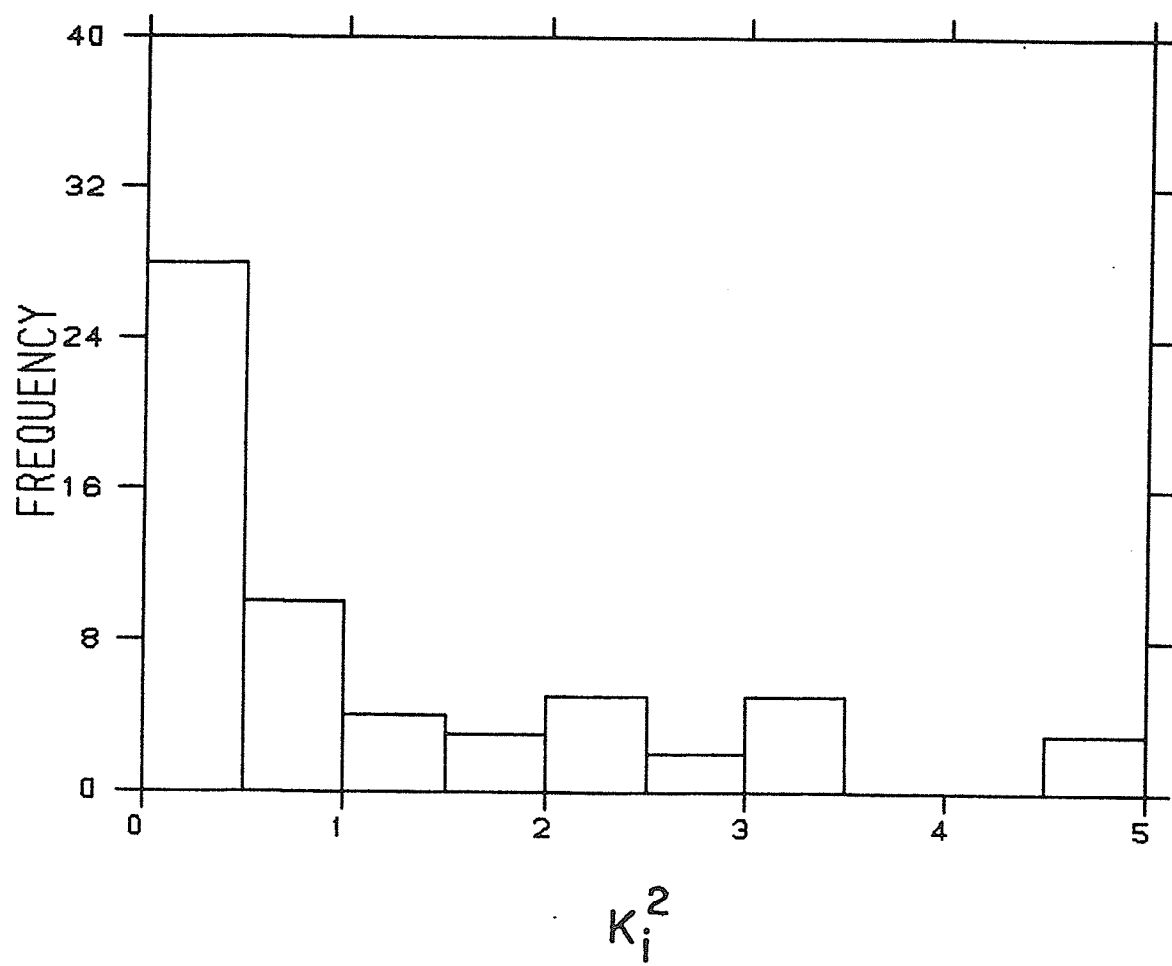
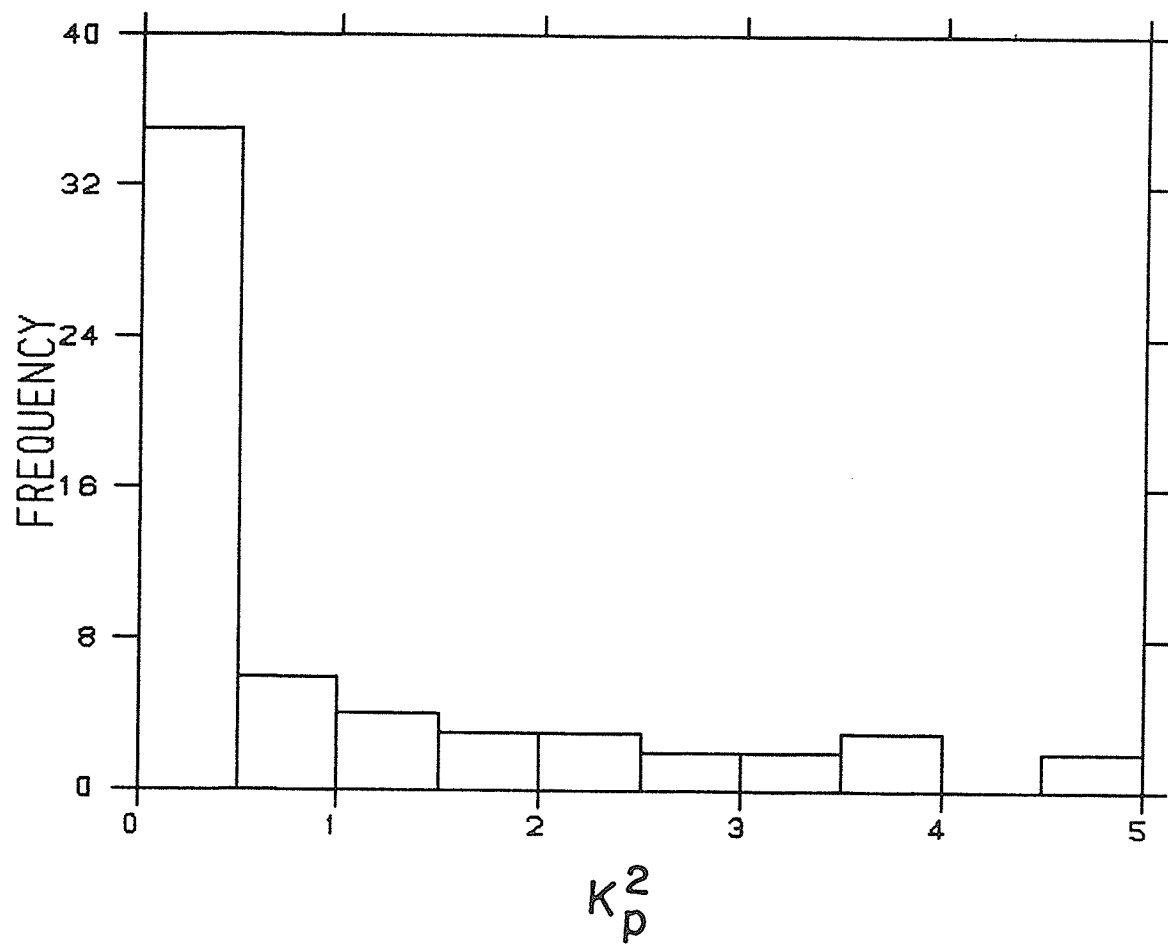


FIGURE 4.5 The distribution of
consistency checks for K_p^2 .



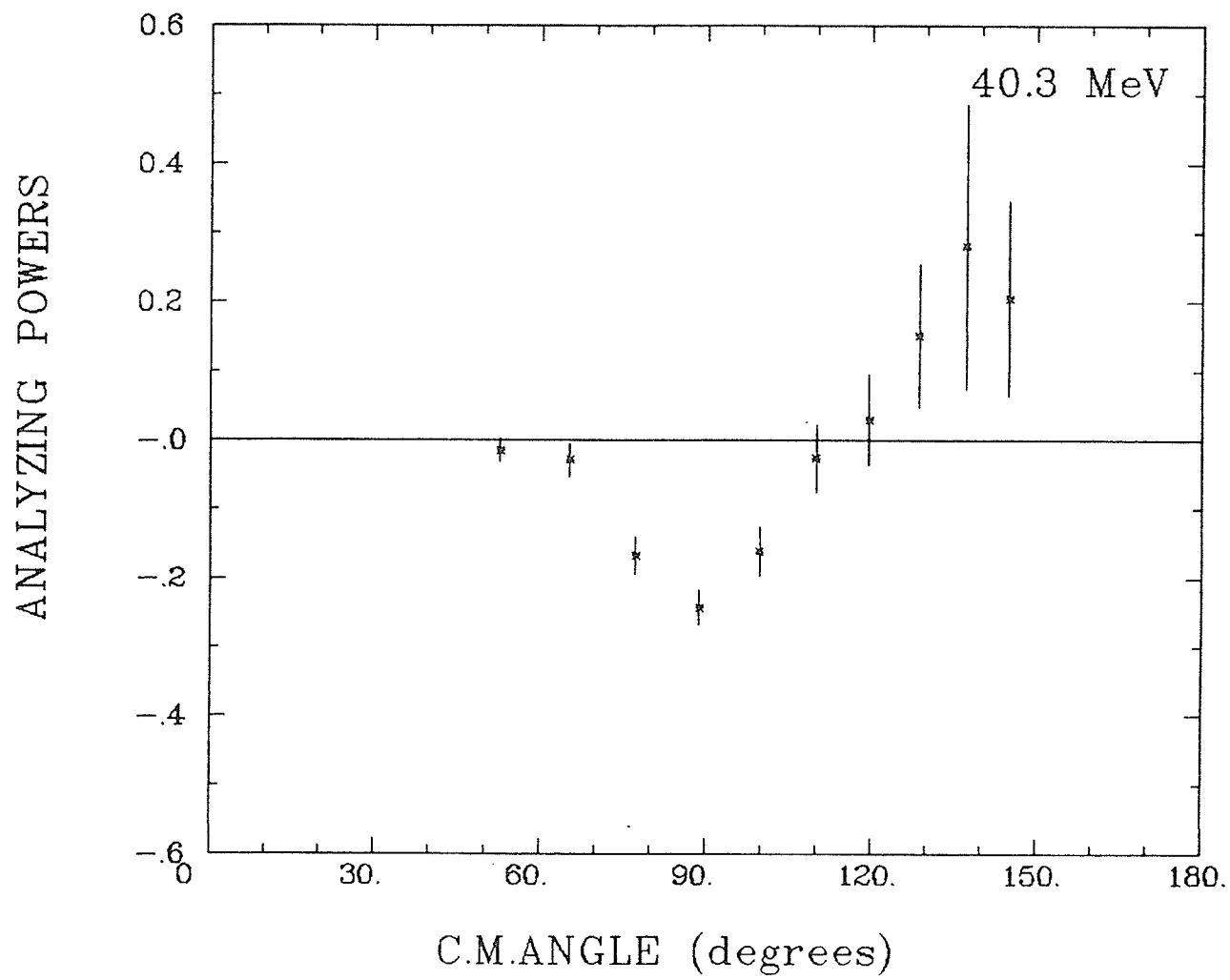
F. RESULTS AND ERROR ANALYSIS

The values of the analyzing powers A_y for protons scattered elastically from polarized Helium-3 are plotted in figure 4.6. Our results for A_y include error bars which reflect the statistical uncertainties in the peak integrations and in the background, as well as the uncertainty in the determination of the beam polarization which was small compared to the statistical uncertainties. The numerical values are listed in table 4.2. These values have been multiplied by the correction factor which is proposed by Verheijen[Ver83]. The data covered angles from 40 degrees to 130 degrees in 10 degree intervals and were taken at the energy of 40.3 MeV.

A total of 15 measurement cycles of four angles each were completed and three more measurement cycles have been attempted. These three measurement cycles had to be rejected due to unstable beam. Counting each angle separately, the actual number of accepted runs was 59 out of 72.

The errors quoted in table 4.2 can be described as, for example, for the angle of 70 degrees the total error is ± 0.026 . This error comprises (i) statistical uncertainties in the peak area and the background which is ± 0.023 , (ii) beam current integration error which is ± 0.0005 , (iii) angle uncertainty which is ± 0.0005 , and (iv) polarization uncertainty which is ± 0.002 . From the above it

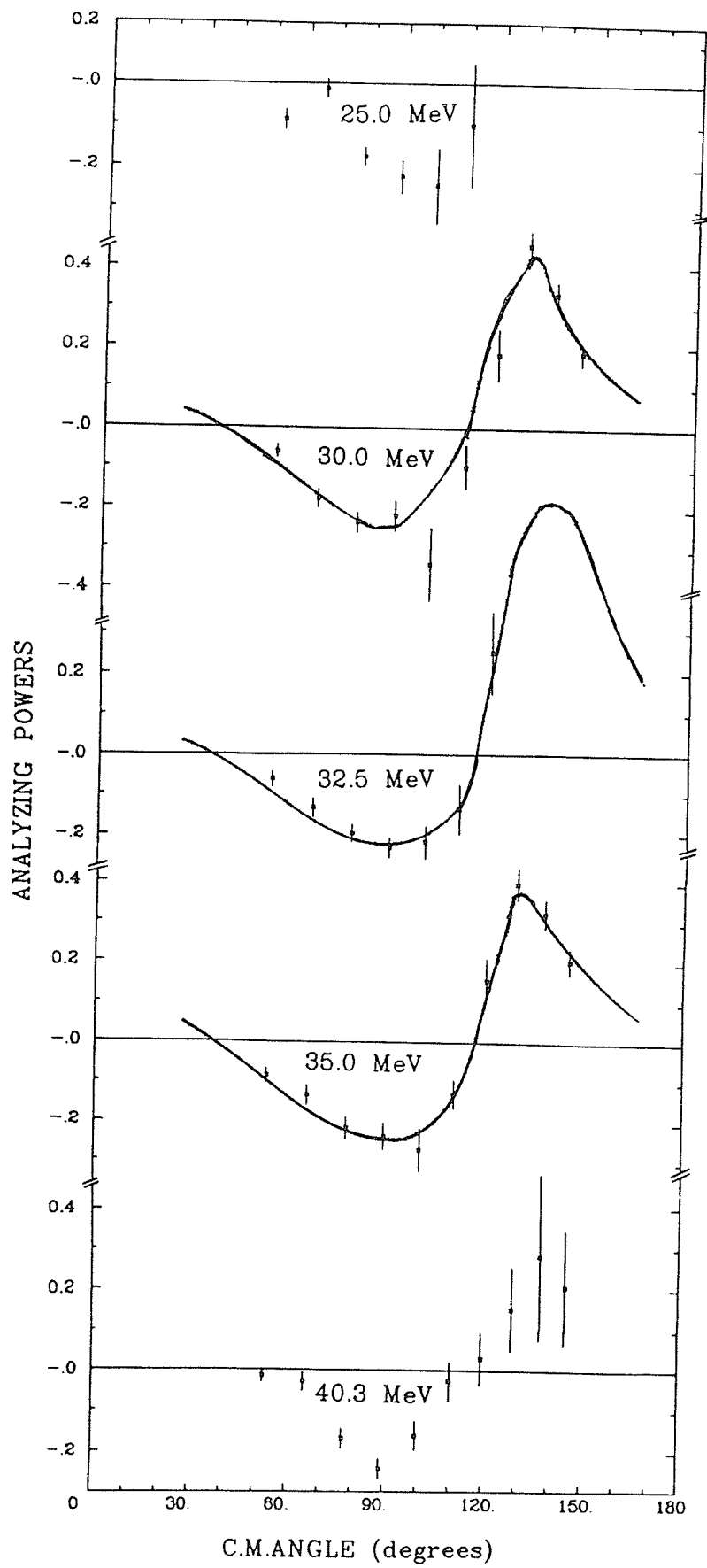
FIGURE 4.6 Helium-3 Analyzing
powers calculated at 40.3 MeV.



Lab angle (deg)	c.m. angle (deg)	Analyzing Powers as from the analysis	Magnetic Field Asymmetry	Instrumental Asymmetry	Correction Factor	Analyzing Powers with correction factor
40.0	52.7	-0.014 ±0.017	-0.049 ±0.010	-0.139 ±0.002	1.04	-0.015 ±0.018
50.0	65.2	-0.029 ±0.025	0.006 ±0.012	-0.109 ±0.003	1.04	-0.030 ±0.026
60.0	77.3	-0.161 ±0.028	0.054 ±0.015	0.029 ±0.003	1.04	-0.167 ±0.029
70.0	88.8	-0.233 ±0.025	0.007 ±0.017	-0.030 ±0.003	1.04	-0.242 ±0.026
80.0	99.6	-0.155 ±0.035	0.009 ±0.027	0.008 ±0.004	1.04	-0.161 ±0.036
90.0	109.9	-0.026 ±0.049	0.100 ±0.039	0.167 ±0.005	1.04	-0.027 ±0.051
100.0	119.6	0.028 ±0.066	0.318 ±0.100	0.127 ±0.007	1.04	0.029 ±0.069
110.0	128.6	0.145 ±0.104	-0.191 ±0.256	0.003 ±0.011	1.04	0.151 ±0.108
120.0	137.1	0.269 ±0.208	0.090 ±0.193	-0.049 ±0.022	1.04	0.280 ±0.216
130.0	145.1	0.198 ±0.141	-0.030 ±0.113	0.102 ±0.012	1.04	0.206 ±0.147

TABLE 4.2 Helium-3 Analyzing powers calculated at 40.3 MeV and asymmetries

FIGURE 4.7 The Helium-3
Analyzing powers as calculated by
Verheijen et al. at 25.0, 30.0,
32.5 and 35.0 MeV, and from this
study at 40.3 MeV.



is obvious that the statistical uncertainty is the determining error, which is also the case for most of the angles.

The normalization error also needs to be taken into account. It is determined mainly by the systematic error in determining the polarization. This method eliminates the magnetic field and instrumental asymmetries up to the first order in their magnitudes. The second order effects are negligible for the above asymmetries compared to the polarization related errors.

Unfortunately a comparison with other data at the same energy cannot be made since other data does not exist at this energy. Figure 4.7 shows the results of McCamis et al.[McC85] at 25.0, 30.0, 32.5 and 35.0 MeV and the results of this study at 40.3 MeV. A phase shift analysis has been made by Verheijen et al.[Ver84] for the 40.0 MeV energy data but with analyzing powers at 35.0 MeV[Ver83] and the differential cross section data at 40.0 MeV[Sou76]. The analyzing powers become slightly more negative at the minimum with increasing energy in comparison with other studies[Ver83].

V. CONCLUSION

A. HELIUM-3 POLARIZATION.

The Helium-3 targets used in the present experiment were built in 1983 at the University of Manitoba, and kept under refrigeration (-20 degrees C). Their performance during the present experiment (1985) was quite satisfactory.

Causes of depolarization were mainly due to relaxation in the presence of a weak discharge, and reabsorption of the pumping light. This can be partially eliminated by covering, with a completely opaque paint, certain areas of the target.

The systematic error in the polarization is mainly dependent on the uncertainties in the geometry factor, and the uncertainty of the absorption factor. A considerable improvement can be achieved by using an alternative measuring method, and by an independent determination of the absorption factor. A probing beam technique for the measurement of the Helium-3 polarization can produce more accurate results than any other method[Dra84]. The various parameters that need evaluation are obtained more easily than the ones required for the method used in this study (fluorescence). Use of both the above methods simultaneously can increase the accuracy and minimize the probable error.

An increase in polarization can be achieved by replacing the discharge lamps with a tunable laser. In principle, many transitions could be utilized for optical pumping (chapter 2.C). The 1.083 micrometers line contains several wavelengths at which optical pumping can be performed. Mollenauer[Mol80] developed an (F_2^+) center laser in NaF which is tunable from 0.99 to 1.22 micrometers with power output of 500 mW. This technology provided the means for improved optical pumping of Helium-3. For a nuclear scattering experiment, the problem appears to be the stability in the intensity of the laser, but it appears to be feasible. The use of a laser can increase the value of P_p^2 on a polarized Helium-3 target by a factor of five (Table 1.1 [Nac82]).

The optical pumping technique can be considered as the best method of polarizing Helium-3, and any further developments should be concentrated on the use of a laser.

B. HELIUM-3 ANALYZING POWERS.

The experimental results for the Helium-3 analyzing powers between 40 and 130 degrees at 40.3 MeV are listed in table 4.2 and are shown in figure 4.6. The Helium-3 Analyzing powers at 25.0, 30.0, 32.5, 35.0 MeV [McC85] and 40.3 MeV [this study] are shown in figure 4.7. The relative errors in the data are given, and are derived from uncertainties in target polarization, beam integration and counting statistics (dominant factor). The instrumental and magnetic field related asymmetries shown in table 4.2 were already eliminated from the results to at least the first order, according to our measurement method, and any second order effects were negligible compared to the other uncertainties.

The data show consistency in the backward angles (greater than 90 degrees), changing sign at a laboratory angle of about 100 degrees to positive analyzing powers, as in other studies [Mul78]. At forward angles (less than 90 degrees), especially the first two angles, the results appear to give small analyzing powers but compare well with those of Verheijen et al. [Ver83] (negative minimum). The consistency tests proved adequate in detecting internal consistencies as described in chapter 4.E. The quality of the results can also be judged from the distributions of the consistency checks.

To complete the Helium-3 measurement project it would be advisable to measure complete angular distributions at 45.0 and 49.0 MeV. A phase shift analysis with the new data is also required as a complement to the overall study. This might help the search involving the A=4 system and might give new and valuable informations.

VI. REFERENCES

- And60: L.W. Anderson, F.M. Pipkin, and J.C. Baird, Phys. Rev., 120, 1279 (1960).
- Bak69: S.D. Baker, D.H. McSherry, and D.O. Findley, Phys. Rev., 179, 1616, (1969).
- Bak71: S.D. Baker, T.A. Cahill, P. Catillon, J. Durand, D. Garetta, Nucl. Phys., A160, 428 (1971).
- Bec75: R. Beckmann, U. Holm, and K. Lorenzen, Z. Physik, A275, 319 (1975).
- Bec77: R. Beckmann, U. Holm, and D. Muller, Nucl. Instrum. Methods, 141, 525 (1977).
- Bir84: J. Birchall, W.T.H. van Oers, J.W. Watson, H.E. Conzett, R.M. Larimer, B. Leemann, E.J. Stephenson, P. von Rossen, and R.E. Brown, Phys. Rev., C29, 2009 (1984).
- Bro78: R.E. Brown, in Clustering Aspects of Nuclear Structure and Nuclear Reactions (Winnipeg, 1978), Proceedings of The Third International Conference on Clustering Aspects of Nuclear Structure and Nuclear Reactions, AIP Conf. Proc. No. 47, edited by W.T.H. van Oers, J.P. Svenne, J.S.C. McKee, and W.R. Falk (AIP, New York, 1978), p.90.
- Bro80: R.E. Brown, B.T. Murdoch, D.K. Hasell, A.M. Sourkes, and W.T.H. van Oers, Internal Report Los Alamos Scientific Laboratory, LA-8179-MS, July 1980.
- Col60: F.D. Colegrove, and P.A. Franken, Phys. Rev., 119, 680 (1960).
- Col63: F.D. Colegrove, L.D. Schearer and G.K. Walters, Phys. Rev., 132, 2561 (1963).
- Dan67: J.M. Daniels, Rev. Sci. Instr., 38, 284 (1967).
- Dan71a: J.M. Daniels, and R.S. Timsit, Can. J. Phys., 49, 525 (1971).
- Dan71b: J.M. Daniels, and R.S. Timsit, Can. J. Phys., 49, 539 (1971).
- Dan71c: J.M. Daniels, and R.S. Timsit, Can. J. Phys., 49, 545 (1971).

- Dra84: P. Drakopoulos, 1984 M.Sc. Thesis, University of Manitoba.
- Fad61: L.D. Faddeev, Soviet Physics-J.E.T.P.,12, 1014 (1961).
- Fia73: S. Fiarman, and W.E. Meyerhof, Nucl. Phys.,A206, 1 (1973).
- Gre64: R.C. Greenhow, Phys. Rev., 136, A660 (1964).
- Kas50: A. Kastler, J. Phys. (Paris), 11, 255 (1950).
- Lal85: F. Laloe, P.J. Nacher, M. Leduc, and L.D. Schearer, in Workshop on Polarized Helium-3 Beams and Targets(Princeton, New Jersey). AIP Conf. Proc. No. 131, edited by R.W. Dunford, and F.P. Calaprice. (AIP New York 1985) p.47.
- Lej74: C. Lejenue, Nucl. Instrum. Meth., 116, 417 (1974).
- McC85: R.H. McCamis, P.J.T. Verheijen, W.T.H. van Oers, P. Drakopoulos, C. Lapointe, G.R. Maughan, and N.T. Okumusoglu, Phys. Rev., C31, 1651 (1985).
- McS70: D.H. McSherry, and S.D. Baker, Phys. Rev., C1, 888 (1970).
- Mol80: L.F. Mollenauer, Optics Letters, 5, 188 (1980).
- Mul78: D. Muller, R. Beckmann, and U. Holm, Nucl. Phys., A311, 1 (1978).
- Mur84: B.T. Murdoch, D.K. Hasell, A.M. Sourkes, W.T.H. van Oers, R.F. Carlson, and R.E. Brown, Phys. Rev., C29, 2001 (1984).
- Nac82: P.J. Nacher, M.Leduc, G.Trenec, and F.Laloe, J. Phys. Lett.(Paris),43, L525 (1982).
- Pet72: D.G. Peterson, Nucl. Instrum. Meth., 104, 451 (1972).
- Rad81: F.N. Rad, R.G. Graves, D.P. Saylor, M.L. Evans, E.P. Chamberlain, J.W. Watson, and L.C. Northcliffe, Nucl. Instr. Meth., 190, 459 (1981).
- Roh71: U. Rohrer, P. Huber, C. Leemann, H. Meiner and F. Seiler, Helv. Phys. Acta, 44, 846 (1971).
- Sch65: L.D. Schearer, and G.K. Walters, Phys. Rev., 139, A1398 (1965).

- Sch84: P. Schmor, Internal Report TRIUMF B.C., TRI-PP-84-42, May 1984.
- Sil59: E.A. Silverstein, Nucl. Instrum. Meth., 4, 53 (1959).
- Smy64: R. Smythe, Rev. Sci. Inst., 35, 1197 (1964).
- Sou76: A.M. Sourkes, A. Houdayer, W.T.H. van Oers, R.F. Carlson, and R.E. Brown, Phys. Rev. C13, 451 (1976).
- Sou77: A.M. Sourkes, M.S. de Jong, C.A. Goulding, W.T.H. van Oers, E.A. Ginkel, R.F. Carlson, A.J. Cox, and D.J. Margaziotis, Nucl. Instrum. Meth., 143, 589 (1977).
- Sza78: G. Szaloky, F. Seiler, W. Gruebler, and V. Konig, Nucl. Phys., A303, 51 (1978).
- Tim70: R.S. Timsit, 1970, Ph.D. Thesis, University of Toronto.
- Tim71a: R.S. Timsit, and J.M. Daniels, Can. J. Phys., 49, 545 (1971).
- Tim71b: R.S. Timsit, J.M. Daniels, and A.D. May, Can. J. Phys., 49, 560 (1971).
- Ver83: P.J.T. Verheijen, 1983 Ph.D. Thesis, University of Manitoba.
- Ver84: P.J.T. Verheijen, R.H. McCamis, P. Drakopoulos, W.T.H. van Oers, J.M. Daniels, and A.D. May, Nucl. Instr. Meth., 71, 227 (1984).
- War75: R.H. Ware, W.R. Smythe, and P.D. Ingalls, Nucl. Phys., A242, 309 (1975).